

Oregon Department of Geology and Mineral Industries  
Open-File Report OFR-O-96-4

Final report  
To  
Bonneville Power Administration  
U.S. Department of Energy  
Portland General Electric Company

Geothermal Resources of Southeast Oregon

Ian P. Madin  
Mark L. Ferns  
Robert Langridge  
A. Mark Jellinek  
Kurt Priebe

submitted by  
Oregon Department of Geology and Mineral Industries (DOGAMI)  
In Fulfillment of  
Agreement DE-B179-91BP19654  
Contract C-94-170780

## Contents

Introduction	2
Photogeologic Mapping and Field Reconnaissance	3
Christmas Valley-Summer Lake	3
Lake Abert	5
Guano Valley	9
Catlow Valley	10
Steens	12
Southern Steens	13
Northern Steens	14
Turpin Knoll	16
Owhyee Uplands	16
Gold Creek	17
Antelope Valley	20
Drewsey	22
Satellite Image Analysis	24
Conclusions	40
References	41
Appendix 1	
Oxygen Isotope Study	
Appendix 2	
Soil Mercury Study	
Appendix 3	
Sawed Horn Geology Map Descriptions	



## Introduction

Recent developments in the energy supply of the Pacific Northwest, such as the continuing controversy over the impact of hydro dams on salmon, and the closure of the Trojan nuclear plant suggest that alternative energy sources may become more economically competitive. Although the geothermal resources of the Oregon Cascades have received a tremendous amount of study, the geothermal resources of southeast Oregon's Basin and Range province (Figure 1) are relatively unknown outside of a few Known Geothermal Resource Areas (KGRA's). The presence of numerous hot springs, high regional heat flow and broad geologic similarities with the geothermal zones of Nevada suggest significant potential, underscored by the attempted development of a resource in the Alvord Desert of Harney County, Oregon by Anadarko. Still, the basic geothermal geology of the region is poorly known outside of the KGRA's, and an improved understanding of this geology could attract significant commercial exploration by identifying new prospects.

The existing database of thermal springs and wells (Figure 1) is sufficient that it is unlikely that any active geothermal systems with shallow manifestations remain undiscovered. It is however reasonable to assume that southeastern Oregon may harbor many blind geothermal systems that do not currently reach the surface. Such systems may however be associated with Holocene or late Quaternary Basin and Range Faulting (such as the Summer Lake KGRA, Alvord KGRA, La Grande KGRA) and complexly and densely faulted Neogene rocks (Crump Geyser KGRA, Vale KGRA). Currently inactive or blind geothermal systems might be expected to manifest themselves at the surface in the form of low-temperature alteration and mineralization zones geographically associated with young or closely spaced faulting. This project attempted to screen large areas of southeast Oregon for such indirect evidence of blind geothermal systems using air photos, satellite imagery and existing geologic data. The project began in 1993, and was funded by grants from the Bonneville Power Administration, U.S. Department of Energy and Portland General Electric. The work was carried out by DOGAMI staff assisted by Dr. Michael Cummings of Portland State University and several graduate student employees of Portland State University, the University of Oregon and University of Idaho. The study covered 11 major regions (Figure 1). In 6 of those areas (North and South Steens, Catlow Valley, Guano Valley, Owhyee Uplands and Lake Abert), air photo fault mapping was focused on major basin margins, and in the remaining 5 (Antelope Valley, Turpin Knoll, Gold Creek, Christmas Lake-Summer Lake and Drewsey) photo mapping was targeted on areas of dense faulting noted on existing geologic maps. Satellite image analysis was carried out for parts of four study areas (North and South Steens, Owhyee Uplands and Drewsey). Most of the areas mapped with air photos or satellite images were visited briefly in the field to determine whether the local geology showed

evidence for blind geothermal systems. Two areas, (Lake Abert and Christmas Lake-Summer Lake) were the subject of more detailed studies of mineralization oxygen isotope geothermometry and soil Hg anomalies. In addition, funds from this project were used to support compilation and publication of numerous previously unpublished temperature profiles for eastern Oregon by Dr. David Blackwell (1995) (~~included as Appendix 3.~~) DOGAMI O-95-03

## **Photogeologic Mapping and Field Reconnaissance**

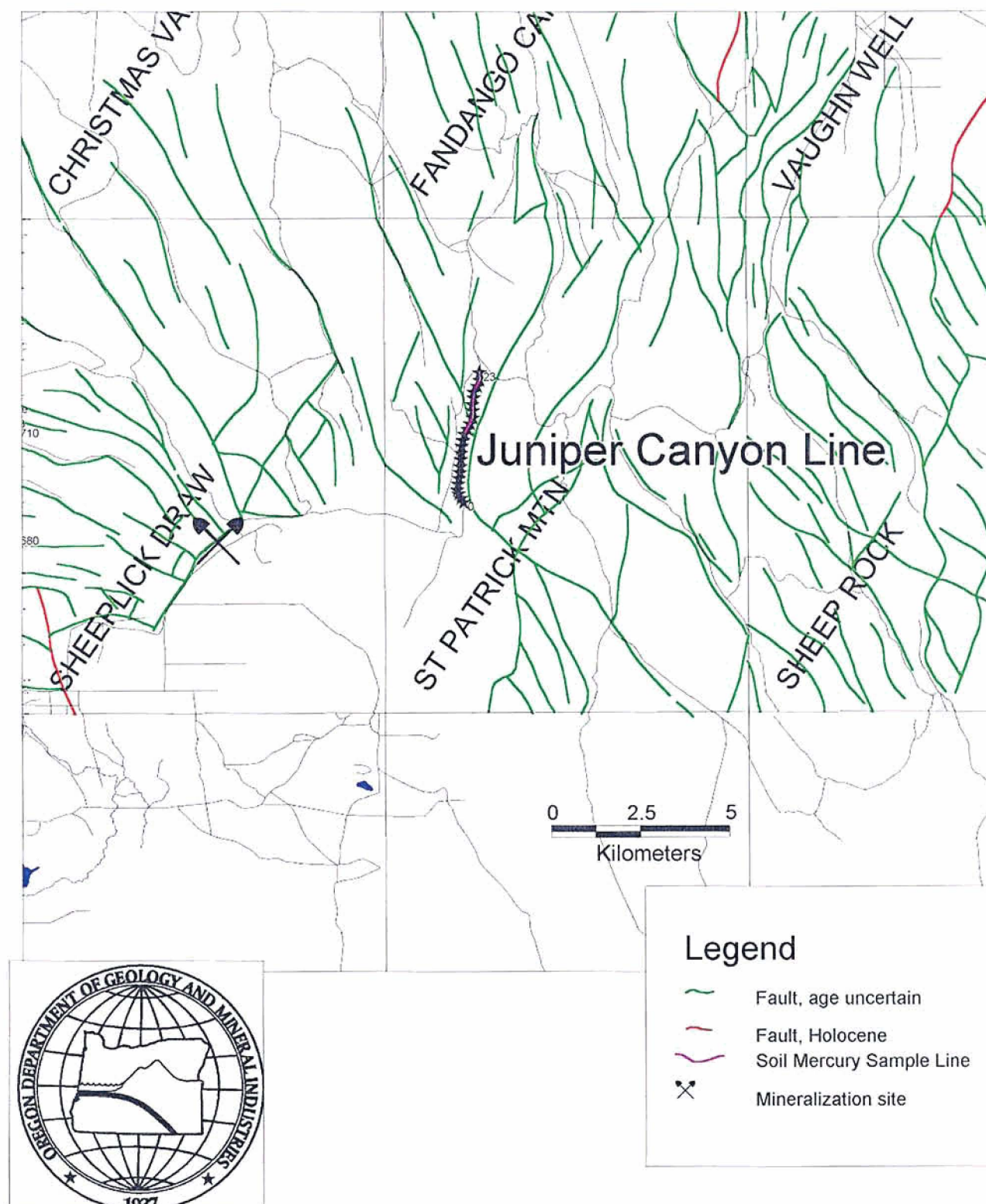
### **Christmas Valley-Summer Lake**

The Christmas Valley-Summer Lake area lies in northern Lake County and occupies the highlands separating the Christmas Lake basin to the north from the Summer lake basin to the south (Figure 1, 2). Geologically, the area consists largely of Miocene basalt flows (Walker and McLeod, 1991) and associated sediments. The area is structurally very complex, cut by NW and NE-trending faults and separating two major structural basins. Faults were mapped by air photo analysis for eight quadrangles in the area (Figure 2,) revealing unusually closely spaced intersecting sets of faults. Field investigation of faults in the study area located only two areas of mineralization likely to be associated with hot springs, one on the Sheeplick Draw Quadrangle in section 22, T. 29 S., R. 17 E (Figure 3), and numerous sites on the Egli Rim quadrangle (Figure 4). Mineralization at the first site consists of travertine cementing late Pleistocene or Holocene pluvial lake beach boulder deposits. The travertine is up to 1-2 cm thick and coats boulders and fills voids between boulders, in some cases with small speleothems growing into large voids. The boulder deposits sit astride one of the numerous faults bounding the northern edge of the Summer lake basin, and it is likely that the travertine was deposited by mineral-rich springs emerging along the fault, like the nearby Ana River springs. There is no data available to suggest that the travertine was deposited by unusually warm water.

The second set of sites (Figure 4) showed abundant  $\text{CaCO}_3$  and  $\text{SiO}_2$  mineralization associated with faults. Mineralization occurred within basalt flows, younger fanglomerate gravels and Holocene colluvium. Mineralization was sampled and analyzed for  $\delta \text{O}^{18}$  values, which indicated that the mineralization was derived from thermal waters with reservoir temperatures possibly as high as 145-205 C. The results of the isotope analysis were published in Oregon Geology (See Appendix 1).

Detailed sampling for soil Hg was also carried out in the Picture Rock Pass area, (Figure 4) but no Hg was detected in any samples. An attempt was made to log a temperature profile in a water well on the Egli Rim quadrangle (Figure 4), but a legal dispute between the owner of the property and his tenant prohibited removing the pump from the well. Access was not possible with the pump in place.

Figure 3. Mineralization site and soil Hg line, Sheeplick Draw and St. Patricks Mountain quadrangles.





This study area shows significant potential for future geothermal exploration. Warm wells are common in both the Summer Lake basin and the southern edge of the Christmas Valley basin, and the area is just north of a geothermal resource area defined by Peterson and others (1982). The complex and closely spaced faulting suggests significant deep permeability is present, and the mineralization suggests that late Pleistocene or Holocene hot springs systems have been active. The absence of warm well and spring data points in the area in comparison to the basins north and south is largely due to the fact that there are very few water wells in the region. This area is a high priority for further exploration, which should include drilling several temperature gradient holes, since the geologic and water well data are favorable and there are no temperature gradient data within 30 or 40 kilometers.

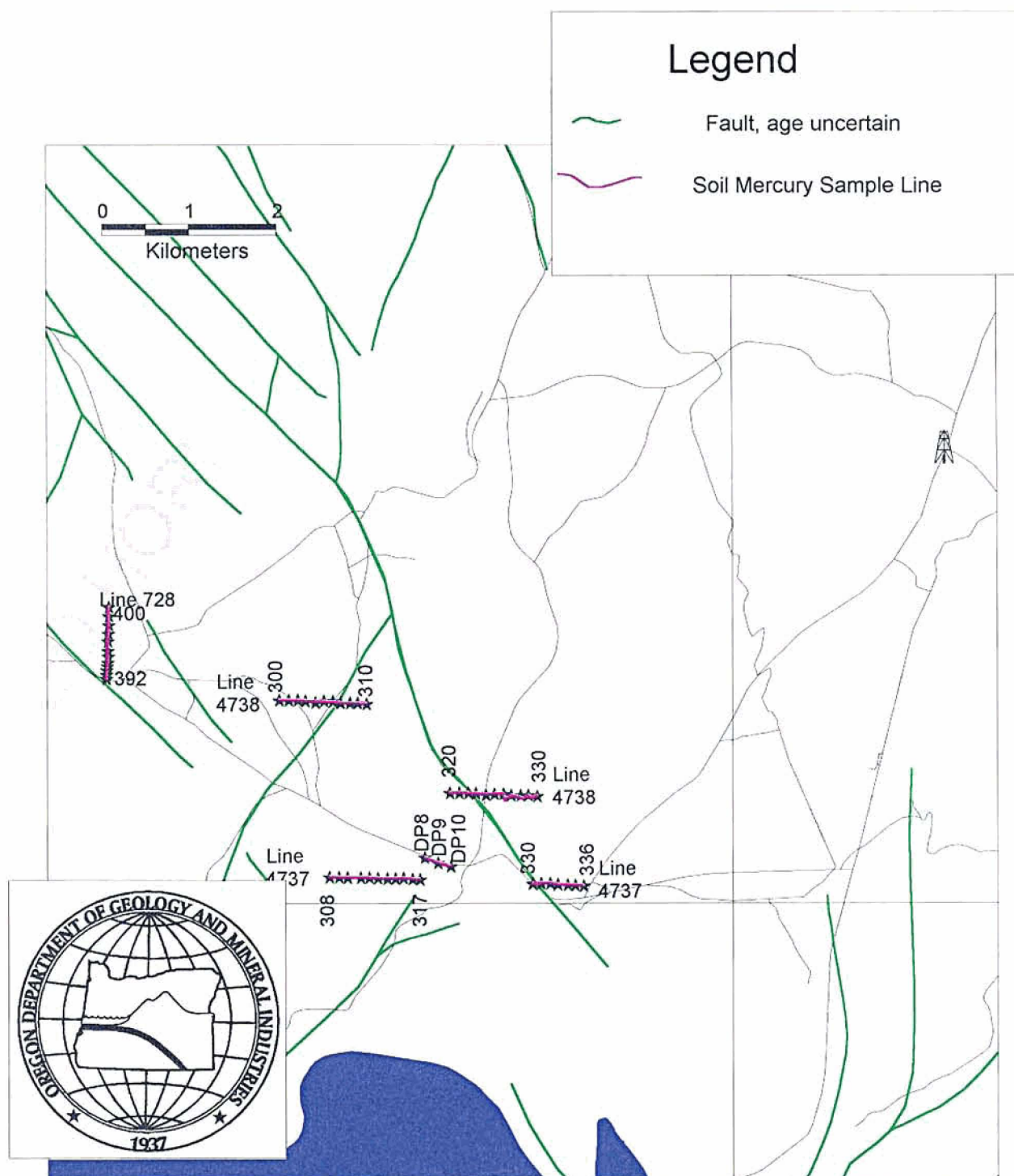
### **Lake Abert**

The Lake Abert area is in central Lake county, and includes the Abert Rim and adjacent Abert graben and Coughlan Hills (Figure 1,5). Lake Abert lies on a downthrown block adjacent to the Abert Rim Fault which exposes a 3,000 ft. Thick section of Miocene volcanics. The lower two-thirds of this section consists of Steens Basalt (14.5-16.0 Ma which were erupted from a large volcanic complex near Steens Mountain, Harney County, and flowed west (Walker and McLeod, 1991). Capping the rim are a series of younger, late Miocene, competent, thinly-layered basaltic lavas. A series of intrusive masses and mafic complexes, most notably the Conley Hills, erupted at a later time, perhaps in association with NW-trending structures. Quaternary sedimentary deposits and Lake Abert dominate the geology of the downthrown block. During the Pleistocene, Lake Abert was part of a larger continuous lake basin called Lake Chewaucan (Allison, 1982), which included the Chewaucan Marshes near Paisley and Summer Lake.

The dominant structural trend (Figure 5) in the area is the NE trending, down to the NW Abert Rim escarpment and associated faults, some of which are Holocene (Pezzopane, 1993). A second trend includes NW trending normal faults with a varied sense of offset which intersect the NE trend, particularly in the Sawed Horn area at the north end of Lake Abert (Figure 6).

Faults along the Abert Rim, near Valley Falls, at the north end of Lake Abert and along the Coglans Buttes were visited in the field to look for evidence of recent mineralization. The only significant mineralization noted was at the Sawed Horn area where there are numerous zones of travertine mineralization (Figure 6). We performed detailed geologic mapping in this area (Figure 6) as well as oxygen and carbon isotope analysis (Appendix 1) of the travertine deposits and soil mercury sampling near some of the faults and travertine deposits (Figure 7). The mapping indicates that the NE and NW trending faults

Figure 7. Soil mercury samples and temperature profile well locations, Sawed Horn area.



are closely spaced and intersecting and probably result in significant fracture permeability at depth. The travertine mounds were almost certainly deposited by mineralized springs emanating into the Quaternary lake Chewaucan. The travertine deposits are associated with faults and the 4300 foot elevation shoreline of lake Chewaucan.

Soil mercury testing was carried out along 5 lines crossing faults or projections of faults associated with travertine mineralization (Figure 7, Appendix 2). Only one line (4737, Figure 7) showed measurable mercury vapor, but at levels comparable to the sensitivity limit of the mercury analyzer used. The remaining lines had mercury levels below the level of detection of the instrument (about 10 ppb). We conclude that there are no significant soil mercury anomalies in the Sawed Horn study area.

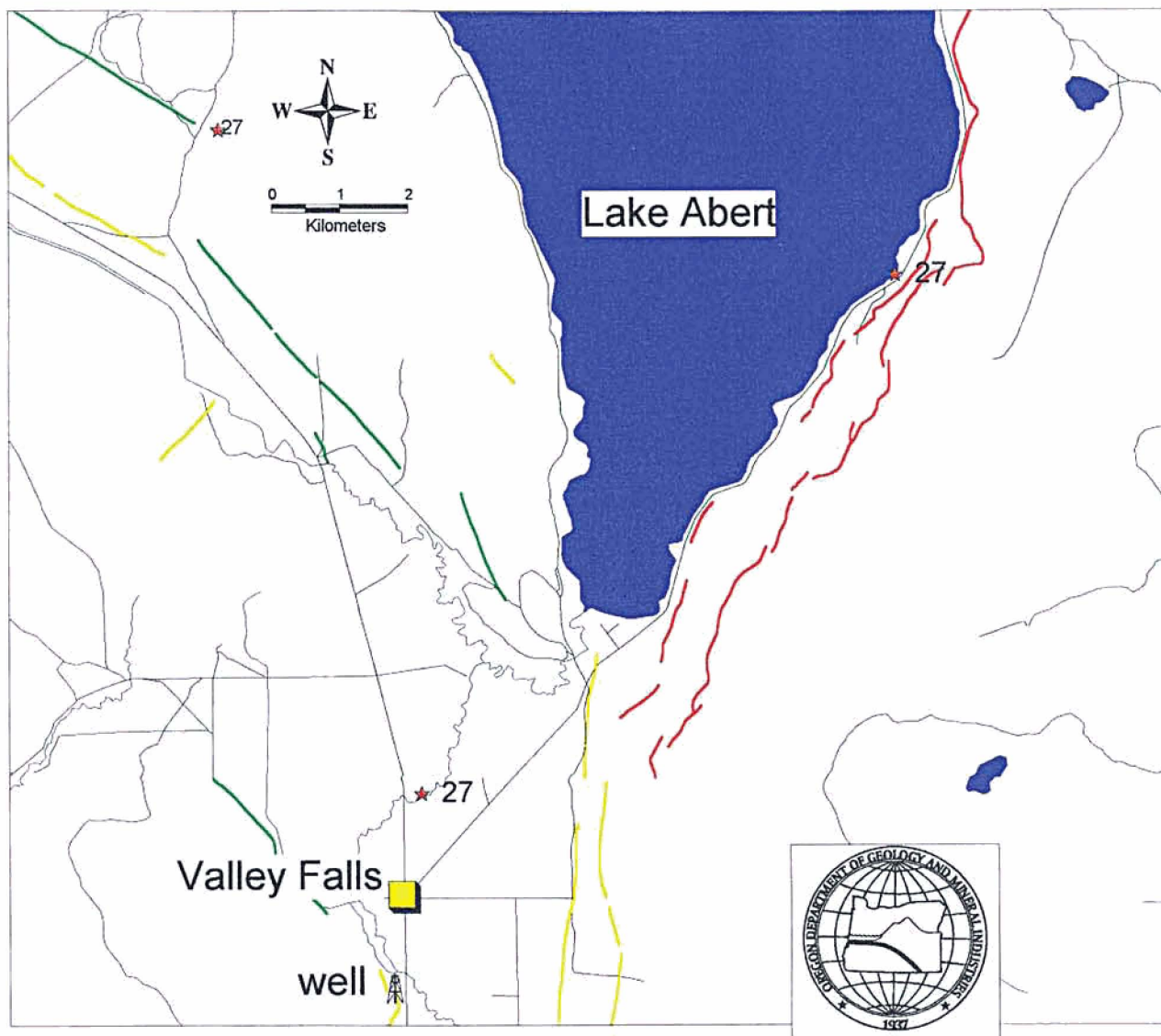
Temperature logs were obtained in the State Block and Euchre wells, located at the east edge of the north Lake Abert area (Figure 5, Table 1). The profile for the State Block well shows a reasonably steady gradient (overall 44 C/km) which is somewhat low for eastern Oregon. The Euchre well although shallow, also shows a reasonably stable gradient (overall 69) and one more typical of southeast Oregon.

Table 1

Temperature Profiles

State Block			Valley Falls			Euchre		
Depth (m)	Temp. (C)	Gradient (C/km)	Depth (m)	Temp. (C)	Gradient (C/km)	Depth (m)	Temp. (C)	Gradient (C/km)
7	11.83		5	10.6		5.0	12.33	0.0
10	12.07	80	10	9.89	-142	10.0	12.80	94
15	12.21	28	15	9.9	2	15.0	13.24	88
20	12.29	16	20	9.9	0	20.0	13.37	26
25	12.47	36	25	9.91	2	25.0	13.62	50
30	12.64	34	30	9.99	16	30.0	14.04	84
35	12.83	38	35	10.02	6	33.0	14.27	77
40	13	34	40	10.2	36			
45	13.22	44	45	10.27	14			
50	13.44	44	50	10.38	22			
55	13.67	46	55	10.53	30			
60	13.94	54	60	10.67	28			
65	14.22	56	65	10.79	24			
70	14.5	56	70	10.95	32			
75	14.76	52	75	11.1	30			
80	14.98	44	80	11.25	30			
85	15.2	44						
90	15.42	44						
95	15.65	46						
100	15.88	46						
105	16.24	72						
110	16.43	38						
115	16.64	42						

Figure 8. Valley Falls area. Well site indicated by grey star. Red stars are thermal wells or springs, temperature in Centigrade. Red lines are Holocene Faults, yellow, Quaternary and green of uncertain age.





A temperature profile was also collected for a well near Valley falls (Figure 8). This well was obstructed at a depth of 80m and yielded a gradient (Table 1) of about 30 C/km, again with probable artesian flow. Other wells in the Valley Falls area produce modestly warm (27 C) water.

There are numerous thermal features in the Abert study area that suggest some geothermal potential. A scattering of warm springs and wells occur along the major fault zones, and there is abundant opportunity for fracture permeability along the Abert Rim fault system and in the intersecting fault zones of the Sawed Horn area. The travertine mineralization suggests that the Sawed Horn area has been the site of earlier hot or warm springs activity. The mercury data suggests that there is no extensive shallow blind geothermal system present. The heat flow data from the State Block and Euchre wells suggests low to moderate heat flow for southeast Oregon. The closest previous heat-flow data point outside the study area is 13 km to the west south of Paisley (Figure 5). The next closest is over 25 km to the southwest. The area has a low to moderate priority for further exploration. Future exploration should include drilling temperature profile holes in the north Lake Abert area or along the Abert Rim.

### **Guano Valley**

The Guano Valley is a north-south trending Basin and Range feature that straddles the Oregon-Nevada border (Figure 1, 9). The valley lacks mapped hot springs, but cross-cutting fault relations and mineralization led us to consider the Guano Valley as a region of potential blind geothermal activity.

Volcanic and sedimentary rocks of Cenozoic age underlie the Guano Valley and surrounding tablelands (Walker and MacLeod, 1991). Over 300 meters of volcanic section is exposed in the Guano and Shirk Rims with basalt flows probably belonging to the Steens Mtn. basalt group (14.7 to 15.5 MA) volumetrically dominant. Locally, ash-flow tuffs and sediments occur within the section, and there are late Miocene basaltic to rhyolitic extrusive centers developed adjacent to regional structures. Beatty's Butte, a large volcanic complex immediately north of Guano Valley has been radiometrically dated at  $10.36 \pm 0.53$  Ma.

Basalts of the rims are competent, and erosion and soil development in tableland environments is minimal. For this reason escarpment retreat may have been the dominant geomorphic agent. Quaternary deposits are largely fault-controlled. The major sedimentary basin in Guano Lake, where fine-grained sediments accumulate between a splay-fault and Shirk Rim. Coarse talus and fan deposits border the range front, but high stand pluvial shorelines and terraces are rarely recognized (Stafford, 1935).

The Guano and Shirk Rims strike N0-20E, paralleling the trend of many of the Basin and Range extension systems in Oregon. The graben widens to the north, but appears to be terminated there against the WNW-striking Eugene-



Denio fault zone (Lawrence, 1976). with limited Basin and Range extension north of this point. They generally strike  $N45\pm5W$  and can be seen cross-cutting tableland blocks.

Numerous faults were mapped on photographs (Figure 9), but no Holocene ground is apparent along either the Guano or Shirk Rims, though it seems likely by the morphology of the escarpments, that Quaternary fault motion has occurred along these faults (Pezzopane, 1993).

Field work was carried out in the Guano Valley to identify areas of mineralization and alteration associated with major faults and zones of intersecting faults concentrated along the Guano Rim and the adjacent tableland and graben areas where uranium and gold prospects occur (Figure 9). Little alteration or mineralization was found during mapping. We conclude that there is little significant hot-springs mineralization associated with faults in this area.

No geothermal gradient measurements had been taken within the Guano Valley region prior to this study (Blackwell et al., 1978), and the closest gradient measurements are in the Catlow Valley (Figure 11), a neighboring Basin and Range system with only moderate heat flow. As a consequence of these data points, the Guano Valley is considered to also have moderate heat flow.

A 600-foot abandoned dry hole was located in the valley near Spalding Ranch. Down-hole heat flow measurement was attempted in this hole, but was unsuccessful. This was because air was being forcibly expelled from the hole from some unknown depth. Obviously there is subterranean fracture of the rocks allowing the active passage of air. Consequently no stable geothermal gradient in still air could possibly be established in the hole.

It would appear that with the data we have, that the Guano Valley area of southeastern Oregon is barren of shallow hydrothermal activity and shows no geologic evidence of blind systems or late quaternary activity. It is highly unlikely that hidden resources suitable for power generation exist, and the area has no population to take advantage of any direct-use resource that might exist. We consider this area to have low potential for undiscovered geothermal resources and does not warrant further work at this time.

### **Catlow Valley**

The Catlow Valley is a low-lying structural basin (Figure 1, 10, 11) bordered on the east by the west-dipping Steens Mountain block, and on the west by the east-dipping Hart Mountain block. The geology of the Catlow Valley is dominated by the flat-floored valley filled by Quaternary and older sediments, and by the surrounding range front blocks of Miocene age (Walker and MacLeod, 1991). The Catlow Rim, which forms the eastern margin of the valley, is dominated by the mid-Miocene (16.0-14.5 Ma) Steens Basalt. A continuous west-dipping block of basaltic flows occur between the Steens Mountain escarpment and the Catlow Rim, broken mainly by a series of discontinuous NW-trending faults. Younger tuffs and sediments overlie this pile

of basalts, and are exposed to the north and southeast of the valley. Younger basalts of Hart Mountain dip eastward toward Catlow Valley, and to some extent must underlie the margins of the Catlow Valley. Rattlesnake Ash-flow tuff (~6.8 Ma) crops out in the north of the valley and was probably also deposited in the valley. At the south end of the Catlow Valley two large silicic volcanic complexes attest to a migration of rhyolitic volcanism in Late Cenozoic times from southeastern Oregon toward Newberry Crater (McLeod et al., 1975) Hawks Mountain ( $13.48 \pm 0.23$ ) and Beatty's Butte ( $10.36 \pm 0.54$  Ma) are large dome complexes of rhyolite decreasing in age to the northeast. During the Quaternary a pluvial lake occupied the Catlow Valley. At least three pluvial shorelines are still visible on the rubble-coated slopes of the Catlow Rim. These features are obvious, but best seen at times of low sun-angle. The central part of the dry lake is largely barren of geomorphic features. Small playa lakes representing remnants of the larger lake occur around the margins, probably near the sites of Late Quaternary subsidence, e.g., Slickey Lake, adjacent to rim faults. Dune fields and marshes are also evident near the margins, the latter being a consequence of springs emanating along the Catlow rim fault.

The Catlow Valley is a structural basin which forms part of the northern Basin and Range in Oregon, and displays faulting in similar orientations to other areas within the Oregon Basin and Range. However, the Catlow Valley does not represent a zone of intense faulting or subsidence, when compared to the Steens and Warner Valley fault systems which border it to the east and west respectively. Along its northern and southern reaches the Catlow Rim, the structure that appears to show the greatest offset, has the typical NNE trend of Oregon Basin and Range systems (Figure 10). At its southern end, offset on the Catlow Rim diminishes, as motion is perhaps transferred to the Guano Valley to the west. A series of long northwest-trending faults (Figure 11) break up the Steens basalt block, and would appear to be important in the structural makeup of the area. One of these zones, of perhaps dextral shear (Lawrence, 1976), known as Long Hollow, is the site for significant mineralization and warm spring activity where it intersects the Steens front. At its northern end the Catlow Rim is terminated by NW-trending faults of the Brothers zone, which dip northward, and effectively separate the Catlow Valley from the Donner and Blitzen Valley by a 400 ft. elevation drop. In its central segment, the Catlow Rim trends NNW. This segment shows the highest escarpments, greatest spring water flow, and least amount of cross-faulting, being dominated by small slump-like faults.

Most of the faults (Figure 10,11) mapped on aerial photographs for this study had previously been documented during geological mapping (see Walker and MacLeod, 1991). Many northwest-trending lineaments were seen within the Quaternary fill of the Catlow Valley, although no Holocene ground rupture is apparent in the Catlow Valley. However, it is likely that Late Quaternary offset or faulting has occurred along the Catlow Rim, and probably also the Fish Fin Rim. The absolute age of most lineaments could not be determined. Photo and ground study suggest that at no time were pluvial shorelines of Catlow lake

offset or disturbed. However, lineaments do appear in fan sediments below these shorelines, and these are commonly mapped as being of higher activity.

Field investigation was carried out to look for mineralization along faults on segments of the Catlow Rim where it was believed that cross-cutting faults and higher density of faults would lead to higher permeability. Mapping was completed at Long Hollow, Dry Creek, and Roaring Springs-Butler Hill along the Catlow Rim. Analysis of fault activity along the rim was also completed along with a study of shorelines. Sparse occurrences of siliceous surface deposits were noted, but significant alteration and mineralization was absent from all mapping areas.

A concerted study of the heat flow within the Catlow Valley by USGS and DOGAMI was reported by Blackwell and others (1978). Several measurements were taken in well holes and drilled holes near the center of the valley (Figure 11). The results of this work suggest that the Catlow Valley is a heat flow depression in the regionally "hot" Oregon Basin and Range. Values measured were in the range 29-63 mW/m<sup>2</sup> (DOGAMI, 1982) suggesting lower heat flow from the crust. This cluster of measurements has regional implications, in that all surrounding areas with no heat flow measurements are contoured according to this depression, e.g., Guano Valley. No heat flow measurements were taken near the Catlow or Fish Fin Rims. Heat flow adjacent to these fault zones could be higher. Due to spring flow along the Catlow Rim, and higher water tables, deep accessible holes are probably not available. No new heat flow data was collected from the Catlow Valley in the course of this study. Down- or through-flow of cold water from the Steens block into the Catlow Valley at may be a cause for depressed heat flow values described above.

Our research and field work in the Catlow Valley would suggest that the region has no obvious manifestations of shallow geothermal systems, blind systems or Quaternary geothermal activity, despite it's proximity to extensive geothermal areas in the Alvord and Pueblo valleys to the east. We feel that this area does not warrant further work at this time.

## **Steens**

The Steens study area consists of two distinct regions, the Southern Steens (Figure 1, 12) characterized by abundant evidence of geothermal activity and Late Quaternary to Holocene faulting and the Northern Steens (Figure 1, 13) with no obvious evidence for either. The two study areas cover the main east-facing Steens escarpment and adjacent valley floor, and share similar regional geology.

The Steens Mountain is geographically the most impressive Basin and Range feature in Oregon, with over 5,000 ft of relief between the Alvord Desert and Steens Mountain summit (9,670 ft). The tilted Steens block exposes a thick section of early Neogene volcanic rocks, which can be subdivided into five main periods and styles of activity, ranging from lower Miocene to Pliocene age

(Walker and MacLeod, 1991). Exposed in gullies near the base of the escarpment are rhyolitic rocks of the Alvord Formation ( $\approx 21$  Ma) and Pikes Creek Formation ( $\approx 18$  Ma). Pikes Creek rhyolite and ash-flow activity is associated with mineralization, which is concentrated along northwest-trending structures that intersect the escarpment and faults.

The bulk of the exposed escarpment section consists of basaltic rocks of the Steens volcano. The Steens Basalts (14.5-16.0 Ma) were erupted from a large shield volcano centered near Steens Mountain. Large volumes of lava were put forth and possibly extend coherently as far west as Abert Rim. Faulting of the volcanic sequence has created the modern Basin and Range landscape. Much of the Alvord Valley and Alvord Desert consists of a broad and gently sinuous plain consisting of Quaternary sedimentary fill and remnant basement slivers. Drainage to the valley is largely internal, and pluvial sedimentation has been an important process in Quaternary times. Quaternary, in some cases Holocene faulting along the southern segment of the Steens escarpment is common (Hemphill-Haley and others, 1989; Pezzopane, 1993), with none noted along the northern segment where extension and sedimentation has not been as dramatic as further south, and much of the downthrown block in the Sheephead Mountains still exposes only Steens basalt.

### **Southern Steens**

The southern segment of the Steens has abundant geothermal features (Peterson and Brown, 1980) (including the largest KGRA in Oregon), numerous Quaternary and late quaternary faults (Hemphill-Haley and others 1989; Pezzopane, 1993) and extensive mineralization associated with range front faulting (Figure 12). Clearly this segment is not a particularly suitable target to search for blind or late Quaternary geothermal systems because there are so many active systems, but it is a useful area to look at for examples of how such systems might manifest themselves in less currently active areas. Accordingly we carried out field reconnaissance to look for alteration and mineralization associated with the faults and lineament mapped on air photos. A total of 17 sites were located with calcite, quartz/chalcedony or zeolite (Figure 12) mineralization. These sites were in addition to the gold, uranium, mercury and copper prospects already identified in the existing mineral occurrence database. In some instances (Alvord Hot Springs, Mickey Hot Springs) there was mineralization in rocks reasonably close to active hot springs. There was however, no obvious mineralization of Quaternary materials except right at the hot springs vents. This suggests that either the vents only affect small areas at the surface, or other Quaternary processes rapidly bury or remove hot-springs mineralization. In either case the likelihood of preserving late Quaternary mineralization in clearly late Quaternary materials in other areas is probably quite low.



## Northern Steens

The northern Steens area (Figure 1, 13) is markedly different from the southern Steens, with far less extension and vertical offset on the Steens escarpment, no hot springs, no Holocene faulting and few mineral occurrences. Still, because it is in the same structural setting as and immediately adjacent to the southern Steens area it is reasonable that it might have evidence of buried or late Quaternary geothermal activity. Numerous Quaternary faults were mapped on air photos (Figure 13), but fairly extensive field checking of the faults and lineaments turned up absolutely no evidence of mineralization or alteration in rocks of any age.

There is no heat flow data available for this study area, although there are high values to the south at the northern end of the Alvord KGRA. There are few warm wells in the area, but it is exceedingly sparsely populated and wells of any kind scarce. Two water wells were logged during the course of this investigation (Figure 13)(Table 2) although both were fairly shallow (Folly Farm 57m, Big Spg C 98 m). Neither well exhibited a steady geothermal gradient, with Folly Farm appearing to have some upward flow of slightly warm water, and Big SpG C showing clear evidence of downward flow of cold water.





Table 2

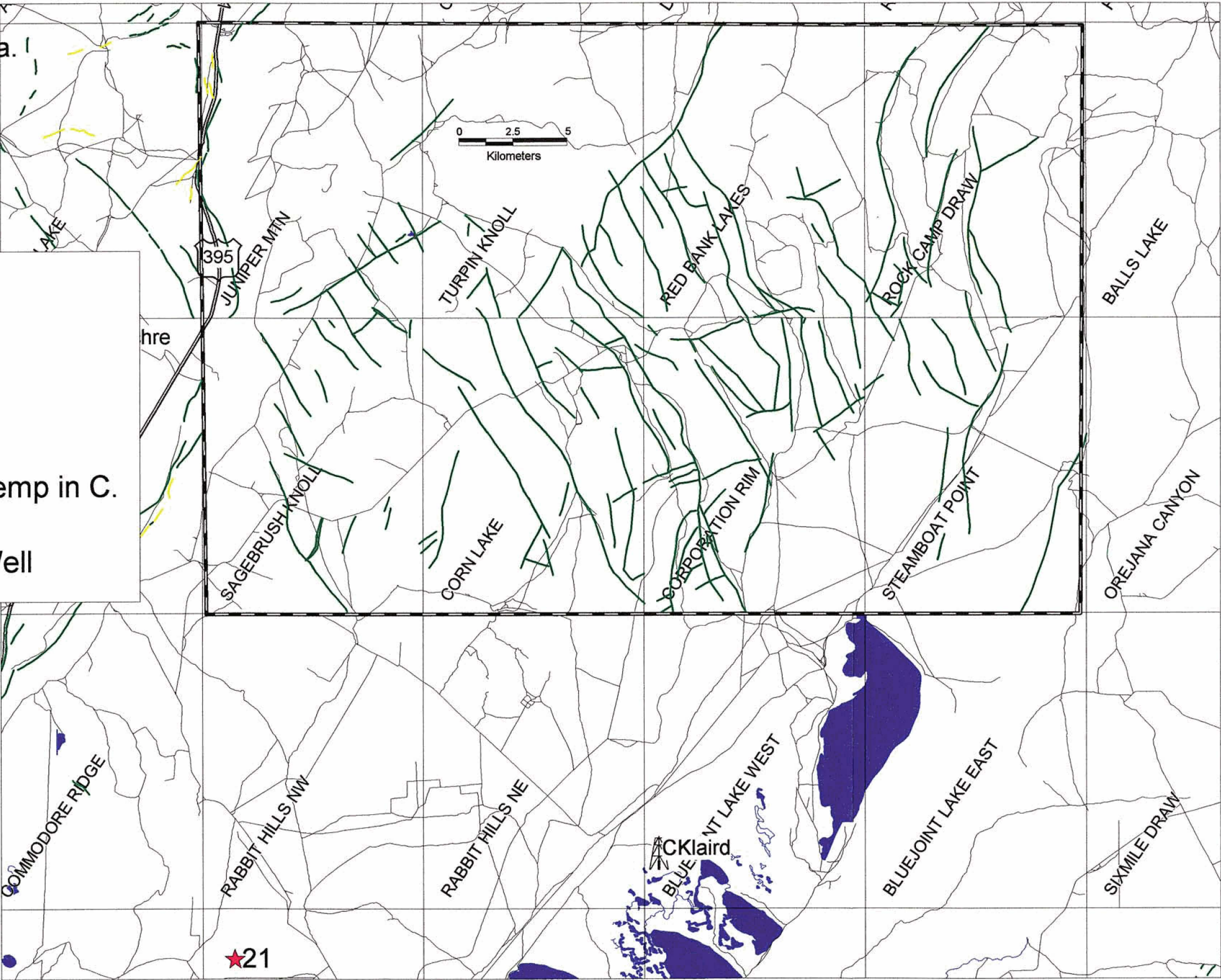
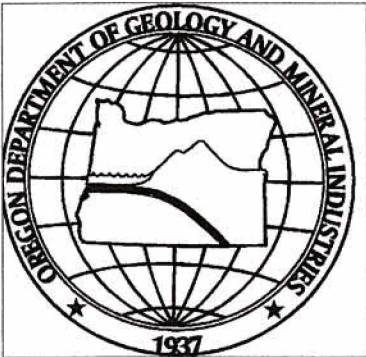
Folly Farm			Temperature Profiles BigSpgC			CKLaird		
Depth (m)	Temp. (C)	Gradient (C/km)	Depth (m)	Temp. (C)	Gradient (C/km)	Depth (m)	Temp. (C)	Gradient (C/km)
5.0	12.37		13.0	13.18		25.0	11.11	
10.0	12.85	96	15.0	13.21	15	30.0	11.15	8
15.0	13.14	58	20.0	13.06	-30	35.0	11.23	16
20.0	13.55	82	25.0	12.95	-22	40.0	11.33	20
25.0	13.98	86	30.0	12.94	-3	45.0	11.47	28
30.0	15.92	388	35.0	12.94	1	50.0	11.65	36
35.0	16.86	188	40.0	12.94	0	55.0	11.8	30
40.0	17.17	62	45.0	12.94	0	60.0	11.85	10
45.0	17.26	18	50.0	12.94	0	65.0	11.87	4
50.0	17.14	-24	55.0	12.95	1			
57.0	17.23	13	60.0	12.96	3			
			65.0	13.00	8			
			70.0	13.03	6			
			75.0	13.05	4			
			80.0	13.14	18			
			85.0	13.25	22			
			90.0	13.40	30			
			98.0	13.41	1			

Figure 14. Turpin Knoll Study Area.

Oregon Department of Geology and Mineral Industries  
Open-File Report OFR O-96-4  
Donald A. Hull State Geoloist

# Legend

-  Fault, age uncertain
-  Fault, Quaternary
-  Warm well or spring, temp in C.
-  Temperature Profile Well





Overall, the northern Steens area shows almost no evidence for the presence of shallow blind or late Quaternary hot springs. It is highly unlikely to conceal a resource as good as that present at Borax Lake, and since there is no population to make use of a direct-use resource, this area is a low priority for further exploration.

### **Turpin Knoll**

This study area was located at the north end of the Warner valley, in an area of complex northeast and northwest trending faults and Quaternary basalt cones (Figure 1, 14). The geology consists largely of Miocene basalt flows and lacustrine sediments overlain by Rattlesnake ash flow tuff (7.05 Ma)(Walker and MacLeod, 1991). The bedrock has been extensively faulted by intersecting NW and NE-trending extensional faults, several of which have served as conduits for later basalt cone eruptions. This area was selected because of the dense faulting and because the southern end of the Warner basin has numerous thermal wells and springs located in the Crump Geyser KGRA, although there are no geothermal manifestations anywhere nearby (Figure 1, 14). We mapped faults on 8 quadrangles in the study area (Figure 14), using air photos. Before visiting the area to look for evidence of Quaternary hot springs mineralization, we had a chance conversation with a geologist from a private geothermal exploration firm who reported that his company had looked at the same area in the past. He reported significant Hg anomalies which led the company to drill several temperature profile holes all of which were reportedly "stone cold". Accordingly, we chose not to pursue further study in this area.

One water well just south of the study area was logged for temperature during this study (Figure 14, CKLaird). The profile is presented in Table 2, and suggests a gradient uncomplicated by groundwater flow, but with a relatively low gradient value (about 20-30 C/km)

This area is probably a very low priority for further exploration, as it is unlikely to have significant blind geothermal systems and has absolutely no population to make use of a direct-use resource.

### **Owhyee Uplands**

This study area includes the highlands and basin and range country south and east of the middle Owhyee river plateau (Figure 1, 15, 16). The area was chosen because of the presence of some hot springs, several warm wells and several moderately high heat-flow measurements and the presence of numerous Holocene and late Quaternary faults.

The generalized geology of the area consists of Miocene lacustrine sediments, basalt and andesite flows and welded ash-flow tuff sheets (Walker and MacLeod, 1991). These bedrock units have been extensively faulted both

along NNW trends associated with Basin and Range extension along the Quinn River valley, and along ENE trends associated with the edge of the Owhyee uplands. Faulted basins are filled with Quaternary fan and playa sediments.

Faults and lineaments were mapped on aerial photographs for 19 quadrangles in the area (Figure 15, 16). Field investigations were carried out to look for mineralization associated with the photographically mapped features for most of the area. A handful of weak to moderate zones of mineralization and alteration were located, typically involving chalcedony veining and bleaching or iron staining of bedrock. None of the areas of mineralization occurred in Quaternary materials, suggesting that this association may not be a very effective tool for locating blind or inactive late Quaternary geothermal systems. In particular, there was extensive alteration associated with the fault immediately adjacent to Easterday hot springs (see section on satellite imagery), but the alteration was restricted to the Miocene bedrock. There was no evidence at this site to suggest that the proximity of the alteration and hot springs is anything but coincidence.

A temperature profile was collected from one water well (Echave) in the study area (Figure 16). The profile shows a strong influence of descending cold groundwater (Table 3) and is of little use in determining whether there are shallow geothermal systems in the area.

Table 3

Echave					
Depth (m)	Temp. (C)	Gradient (C/km)	Depth (m)	Temp. (C)	Gradient (C/km)
3.0	12.95		60.0	11.92	-1
5.0	12.68	-133	65.0	11.90	-4
10.0	12.00	-136	70.0	11.85	-9
15.0	11.98	-5	75.0	11.81	-9
20.0	11.97	-2	80.0	11.77	-8
25.0	11.96	-1	85.0	11.74	-5
30.0	11.97	1	90.0	11.71	-7
35.0	11.97	1	95.0	11.68	-5
40.0	11.97	0	100.0	11.65	-7
45.0	11.95	-4	105.0	11.60	-9
50.0	11.93	-4	110.0	11.56	-8
55.0	11.92	-2	115.0	11.52	-8

Although it was not possible to locate significant hot-springs mineralization in Quaternary materials associated with the many young faults in the Owhyee uplands study area, it is still likely to be an area of significant potential. Previously measured heat flow values are high (71-213 mw/m<sup>2</sup>) and extensive faulting provides the opportunity for significant fracture permeability. This area should be considered a moderate to high priority for further investigation, with gradient hole drilling the next step to test the association of high heat flow and young faulting.



## Gold Creek

The Gold Creek area is located adjacent to Highway 20 and the Malheur River gorge, in Malheur County, Oregon (Figure 1, 17). Alteration, mineralization and active geothermal activity have been recognized at this location. A series of small hot springs delineate an unmapped geothermal site here named "Oxbow" Hot Springs", which may have resource potential although currently a Wilderness Study Area designation has been placed on the hills to the south of the Oxbow Hot Springs.

Recent geological mapping was completed for the South Mountain sheet (Evans, 1990) in which the Oxbow Hot Springs occur. Rocks of the Gold Creek area and Malheur Gorge are of Miocene age or younger, and consist largely of volcanic rocks and their sedimentary associates. Mid-Miocene volcanism in the area was bimodal (basalt-rhyolite) in nature and probably related to Columbia River basalt extrusions and Basin and Range igneous activity.

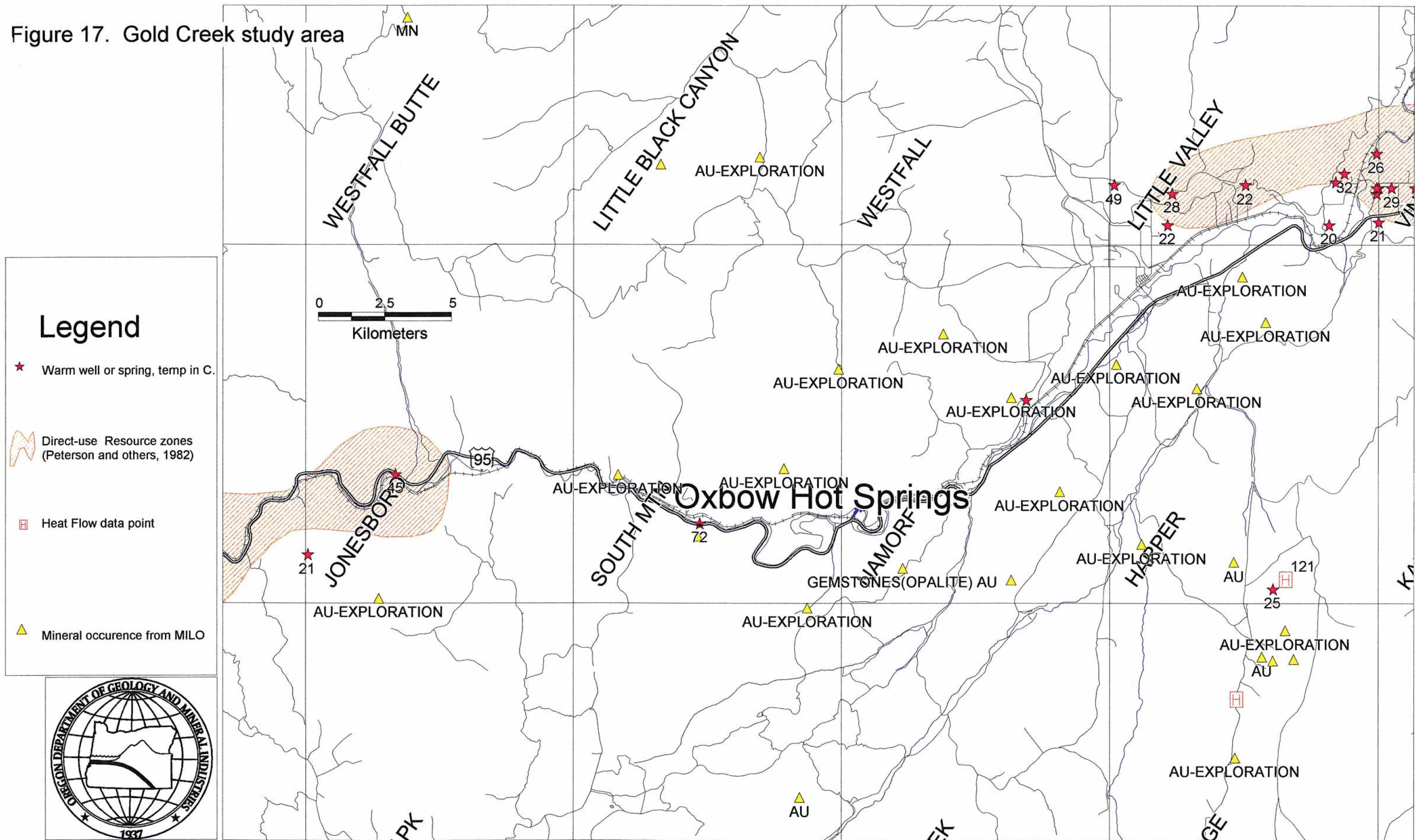
Stratigraphy on the south side of the river consists almost entirely of Miocene basalts (Malheur Gorge basalt; Evans, 1990), cross-cut by alteration and veining. On the north side of the river there is a prominent ash-flow tuff unit (Dinner Creek Welded Tuff; 14.9 Ma).

A number of veins associated with a hydrothermal system were mapped. One in particular is a two meter wide gold-bearing quartz vein with positive relief that is exposed for nearly 800 m and trends N45W, parallel to the alignment of the several vents making up the hot springs. Apparently geothermal activity has been active both during the Miocene to produce the quartz vein and again during the Quaternary to produce the active hot springs. Despite the fact that both appear to be aligned with NW trending faults mapped by Evans (1990), the association may be coincidental.

The Oxbow Hot Springs are a linear series of springs within an old meander oxbow of the Malheur River. Although mentioned by Evans (1990), the Oxbow Hot Springs have not been described in accounts of Oregon geothermal studies (Peterson and others, 1982). The springs lie above the south bank of the modern river, nestled against fan deposits and bedrock and range in temperature from 44°-72°C. The hottest of these springs is centrally located, and has an actively forming silica and carbonate sinter sheet, with nodular silica growths around and near spring outlets. At other springs there are generally uncemented hot spring deposits, rich in algal mat material. The waters may contain a significant amount of biochemical toxin, e.g. Hg, As, Sb because spring deposits have held back marsh grasses. Blocks of quartz vein eroding out of fan sediments and possibly directly from the vein upslope are being incorporated in the hot spring deposits along with other large clasts.

Analysis of aerial photographs showed a paucity of lineaments that exhibit potential for active faulting. Most fan surfaces are uncut by faults.

Figure 17. Gold Creek study area





However, near river level there are northwest-trending features associated with the hot springs and veins. It is apparent that NW-trending faults are the dominant Quaternary structures in this region, and where intersections with northerly-trending "Basin and Range" faults occur, there is potential for permeability and hot spring activity.

The immediate area contains numerous hot springs, warm wells and elevated heat flow data points (Figure 17), although there are no gradient holes near the site. This area is a moderate to high priority for further exploration, although the wilderness study designation complicates exploration, and the well characterized KGRA at Vale to the east overshadows the importance of the Gold Creek area. Further exploration should involve gradient hole drilling to test the association of the NW trending faults with high heat flow and permeability.

### **Antelope Valley**

The Antelope Valley area is located in far eastern Oregon just south of the community of Jordan Valley (Figure 1, 18). The local bedrock geology consists of Miocene basalt flows, lacustrine sediments, rhyolite flows and plugs, and extensive Quaternary and Holocene basalt flows (Walker and McLeod, 1991). The Antelope Valley occupies an east-west trending graben whose southern border is a major east-west fault zone and whose northern margin is buried beneath the young basalt flows. The area was chosen because of the presence of the graben bounding fault, associated with several sites of gold mineralization and a scattering of hot springs and wells and high heat flow values (Figure 18).

Faults and lineaments were mapped using air photos along the southern border of the Antelope valley graben, informally named the Parsnip Peak fault zone. Reconnaissance mapping was carried out along the fault zone to look for areas of Quaternary hot springs mineralization associated with the faulting. Mapping identified a previously unmapped major anticline south of the Parsnip Peak Fault zone. The anticline axis trends north along Lone Tree creek, right along the Oregon Idaho border, and is truncated by the fault zone. The east limb dips about 20-25 degrees east and the west limb 20-25 degrees west. A major fault runs down the anticline axis.

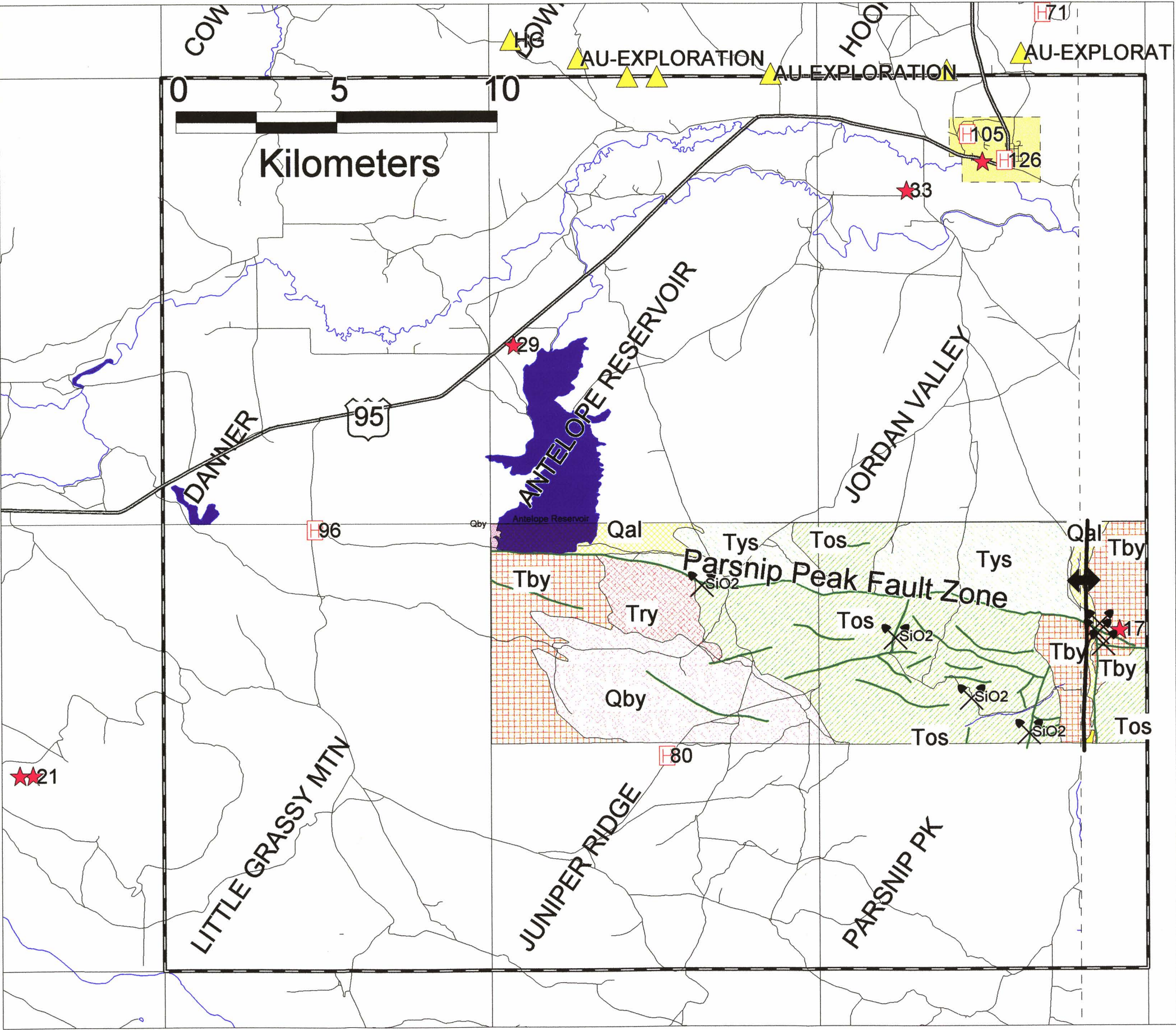
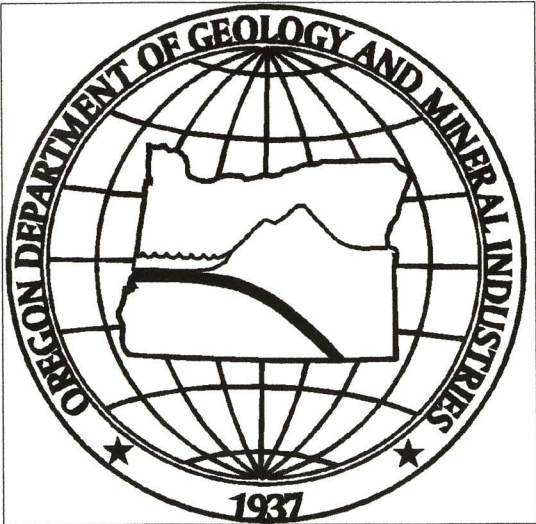
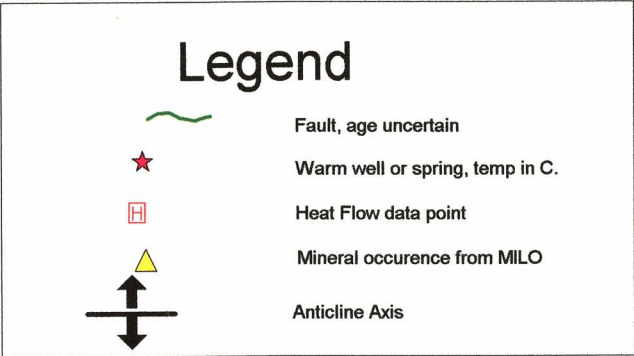
Numerous areas of significant SiO<sub>2</sub> mineralization of bedrock units were located (Figure 18), but no mineralization was noted in Quaternary materials. Mineralization appeared to be associated with major faults or intersections of faults. Extensive mineralization was located at the intersection of the Parsnip Peak Fault Zone and the axial fault of the major anticline. In addition, there is an uncatalogued warm (17.3 C) spring at the intersection. All the other spring temperatures measured in the area had temperatures ranging from 7 to 10 degrees C, so the 17 degree spring is a significant local anomaly.

The Antelope Valley area has a moderate to high priority for further exploration. There is good evidence that the Parsnip Peak Fault Zone has



Figure 18. Antelope Valley study area.

Geologic Units: Qal= Quaternary Alluvium, Qby= Quaternary Basalt, Tby= Miocene Basalt, Try=Miocene Rhyolite, Tys=younger Miocene lacustrine sediments with basalt and rhyolite, Tos=older Miocene lacustrine sediment with basalt and rhyolite.





channeled pre-Quaternary hot springs fluids, and the anomalous spring described suggests that this may still be the case. In general the area has fairly high (71-105 mw/m<sup>2</sup>) heat flow values, a significant number of warm wells and springs and some of the most extensive and youngest basalt eruptions in Oregon. Further exploration should involve drilling gradient holes along the Parsnip Peak Fault zone.

### **Drewsey**

The Drewsey area is located to the northeast of the Harney Basin along the upper reaches of the Malheur River (Figure 1, 19). The area was chosen because of the presence of scattered warm springs and wells, a few high heat flow data points and the presence of significant faulting and some gold and mercury prospects. The geology of the area is very complicated, bedrock units are typically volcaniclastic medium to fine grained fluvial and lacustrine sediments interlayered with ash flow tuffs, basalt flows and rhyolite plugs (Walker and McLeod, 1991).

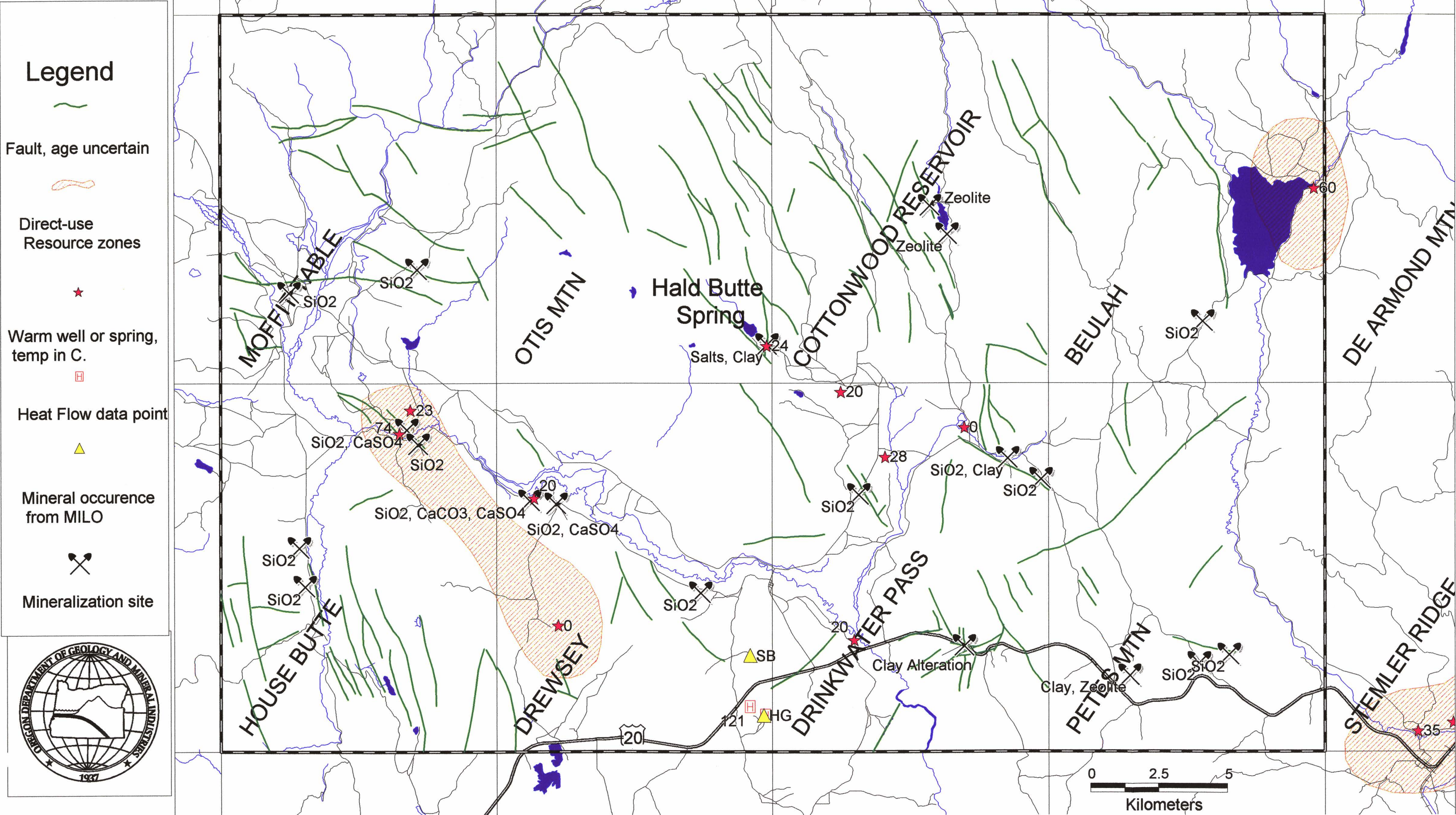
Faults were mapped using aerial photography and field reconnaissance was carried out to look for alteration or mineralization of Quaternary rocks in association with the faulting. In addition to examining faults for evidence of mineralization, the field work discovered a previously uncatalogued warm spring (24 C, Figure 19).

Numerous sites of alteration and mineralization were located. Alteration zones typically involved bleaching of lava flows or debris flows and conversion of original mineralogy to clay with deposition of clays and zeolites in voids and fractures. Mineralization zones typically involved opaline or chalcedonic silica, sometimes in association with calcite and gypsum. With one exception (see below), all the mineralization observed (Figure 19) occurred in Miocene age rocks. One spectacular example occurred in basalt flows immediately adjacent to the Drewsey Hot Spring (Figure 19, 74 C). The basalt is extensively bleached or stained green, with extensive mineralization of opal, chalcedony and gypsum in fractures vesicles and voids. Although there is no evidence for the age of alteration of the basalt, it is possible that the Drewsey hot spring has been sufficiently long lived and hot to have caused the mineralization. Both the springs and mineralization fall on NW trending faults.

The one site in which mineralization was not in Miocene rocks occurred in the area immediately adjacent to the newly catalogued warm spring. Colluvium on slopes within a few tens of meters of the spring is suffused with white mineral salts of unknown composition, and basalt and rhyolite clasts are partly altered to clay. This site is instructive, because it is one of the few instances in the course of this investigation where mineralization and alteration in Quaternary materials was clearly associated with geothermal activity. This relatively diffuse alteration zone might easily be overlooked in the absence of the warm spring, because similar salt accumulations are common in arid regions, and the clay alteration is



Figure 19. Drewsey study area.





not particularly spectacular. The alteration and mineralization associated with this spring suggests that the temperature has always been fairly low, without widespread deposition of silica. Such weak surficial manifestations of Quaternary geothermal systems are probably highly unlikely to be well preserved or recognizable.

The geothermal potential of this area is suggested by the presence of numerous warm springs and wells, as indicated by the geothermal resource zone designated by Peterson and others (1982)(Figure 19). This investigation supports that designation, and possibly suggests that the area may have even more potential. Although the number of warm wells in the area is small, there are very few wells at all, and the proportion that are warm is significant. In addition, the area has abundant shallow groundwater and cold springs fed by the highlands to the north, which probably obscure part of the geothermal activity. Faulting in the area is locally very closely spaced and complex, but in much of the area it is not possible to resolve the structure from air photos and reconnaissance. This area is a high priority for further exploration which should include detailed geologic mapping and drilling of geothermal gradient holes, particularly on the Otis Mountain and Cottonwood Reservoir quadrangles.

### **Satellite Imagery analysis**

Landsat thematic mapper (TM) imagery was examined for a large area of southeast Oregon (Figure 1) in order to determine whether mineralization around active hot springs could produce a signal that could be used to rapidly search for inactive hot springs over large area. In order for this to succeed, several conditions must be met. First, the mineralization must be sufficiently widespread to cover several satellite image pixels (nominally 30m by 30m). Second, the mineralization must be relatively persistent, so that the associated signal is still visible after hundreds or thousands of years. Third the signal produced by the mineralization must be relatively unique, otherwise searches of large tracts will return a high number of false targets. Finally, the signal due to mineralization must not be masked by signals due to vegetation, a serious problem with hot springs in arid environments.

### **Image processing procedure**

Imagery was obtained from the US Geological Survey in the form of 8mm tape cartridges carrying seven bands of data for each quarter scene. The Imagery was converted from 8 mm to DC2120 tape format by the Oregon Service Center for GIS, and then read directly off the tapes using IDRISI (Clark College, 1990, 1995) a raster-based image analysis and geographic information system software package. Mapinfo™ mapping software was also used for image registration and viewing.

## **Georeferencing**

Bands 1-5 and 7 of the Landsat data were used, each with a nominal resolution of 30 m. Band 6, the thermal infrared band has a resolution of 120 m and was not used. For each quarter scene of interest, all 6 bands were first roughly georeferenced by resampling with four correlation points. The roughly georeferenced images were then viewed with Mapinfo in order to pick a larger number of correlation points for smaller sub-areas of the image. These correlation points were then used to accurately georeference small areas of imagery corresponding to 1:24,000 scale topographic maps. The georeferencing generally resulted in registration errors of 1 to 2 pixels (30 to 60 m).

## **Normalization**

Within each band, the imagery simply records the relative brightness of each pixel. Part of this signal is due to the character of the material at the site, and part is due to the relative strength of illumination of the site, a function of sun elevation, azimuth and topography. In order to examine the spectral signature of the images surrounding active hot springs, the images were normalized to remove the effects of uneven illumination related to topography. US Geological Survey 7.5 minute Digital Elevation Models (DEM's) were obtained for the quadrangles containing the target active hot springs. From each DEM, relative illumination was calculated using sun elevation and azimuth data for the image in question. The relative illumination data was then used to normalize each band of imagery for the quadrangle in question.

## **Analysis**

For each active hot spring area studied, the normalized bands were combined into three band composites using all possible combinations. This produced a total of 20 composite images. Each of these images, and the six single-band images from which they were derived was then automatically classified into groups of similar values, and each group was labeled according its frequency of occurrence in the image. This procedure has the advantage of providing images which display the degree of uniqueness of a particular site. Each of the classified images was then viewed to determine whether there were any pixels adjacent to the active hot springs which were highly unique (> 95th percentile) for that image. For each active hot spring the images with the most unique pixels in the hot springs area were then combined to determine which areas shared the highly unique values. The characteristics of these highly unique areas around the active springs were then used to search composite images of large areas (30 minute by 30 minute or quarter-scene) for similar



characteristics. This technique is entirely empirical, no attempt was made to match spectral characteristics of potential target minerals with the imagery.

## **Results**

### **Easterday Hot Springs**

Easterday hot spring is located on the Boghole Springs 1:24,000 quadrangle, near McDermitt, Nevada (Figure 1,16,20). The spring emerges in colluvium covering a fault which separates a bedrock high to the east from playa and fan alluvium to the west. The area immediately west of the spring is covered with marsh and salt marsh vegetation watered by the spring. Several prospects in the bedrock reveal jasperoid silica mineralization.

Although there were areas of quite unique spectral characteristics in the marsh area west of the spring, there were only a few pixels with unique spectral characteristics in the colluvium/bedrock southeast of the spring. These areas were extremely unique on the Band 135 and 357 composite images. Accordingly the values for those pixels from the two composite images were used to search. Band 135 and 357 composites of the west half of the Louse Canyon 1:100,000 sheet were searched using the Easterday springs characteristics. A total of 355 pixels out of 2,242,038 (0.015%) were identified as matching both the Band 135 and Band 357 composite values, and defined 14 target areas (Figure 20). All geology for the following target descriptions is from Walker and MacLeod, 1991.

One group of targets occur in the NW corner of the Battle Creek Ranch Quadrangle, in Section 19 and 30 of T. 35 S., R. 41 E. and Section 36, T. 35 S., R. 40 E.. All of these targets are on bedrock slopes underlain by basalt flows.

Another group occurs on the northern edge of the Blue Mountain Pass quadrangle and southern edge of the Basque quadrangle. One is located in Section 17, T. 37 S., R. 42 E. in bedrock mapped as (Twt of Walker and McLeod, 1991). The others are located in Section 17 and 8 of T. 37 S., R. 42 E., in bedrock mapped as basalt.

Another group occurs at the northern edge of the Blue Mtn. Basin quadrangle and the southern edge of the Three Man Butte quadrangle, in section 23, T. 36 S. R.40 E., section 24, T. 37 S. R. 40 E., and sections 7, 8, and 17, T. 37 S. R. 41 E.. These targets occur on bedrock slopes mapped as welded tuff.

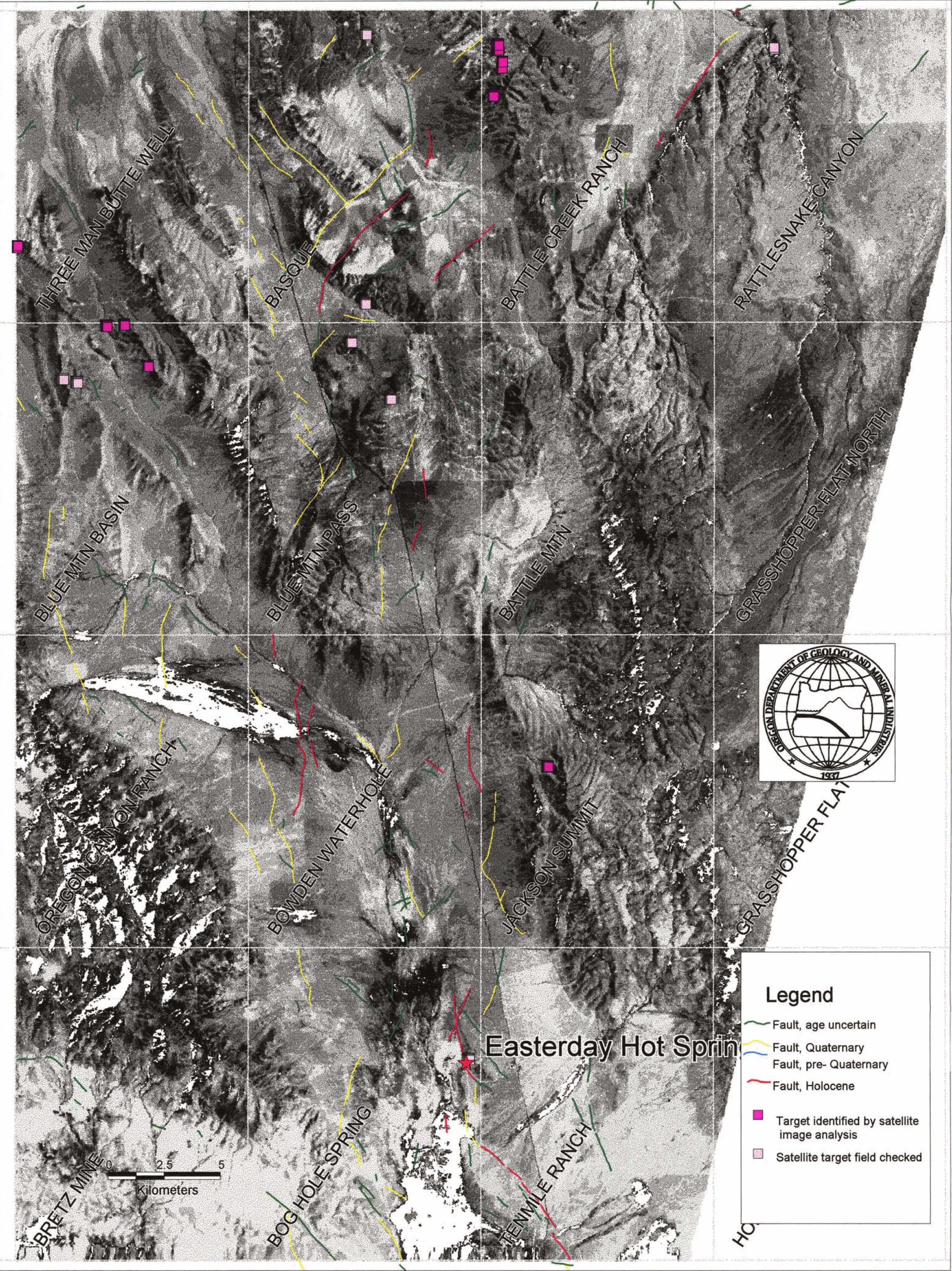
A target occurs on the Rattlesnake Canyon Quadrangle I section 19, T. 35 S., R. 42 E.. The bedrock at the site is mapped as rhyolite flow or tuff.

A target occurs on the Basque quadrangle in section 21, T. 35 S., R. 40 E.. The bedrock at the site is mapped as ash-flow tuff.

A target occurs on the Jackson Summit quadrangle in section 7, T. 39 S., R. 43 E.. The bedrock at the site is mapped as ash-flow tuff.



Figure 20. Louse Canyon West Satellite Image





## Alvord East

The Easterday Hot Spring search criteria were applied to the east half of the Alvord Lake 1:100,000 quadrangle (Figure 1, 21). This search returned 2,808 out of 2,529,474 pixels, a much higher percentage (0.111%) than for the west half of the Louse Canyon sheet. There are too many pixels to describe individually, all are depicted in Figure 21. Several important groups stand out.

Group 1 is located on the Tule Springs quadrangle, in sections 15, 21, 22, 23 and 28 of T. 35 S., R. 35 E.. These pixels are aligned along a major fault (Walker and MacLeod, 1991) separating basalt (unit Tba) from dunes and playa alluvium.

Group 2 is also on the Tule Springs quadrangle, in sections 15, 16 and 17 of T. 36 S., R. 35 E.. Geology of the area is ash flow (Twt) and basalt flows (Tb), and there are numerous faults.

Group 3 is located on the Tule Springs NE quadrangle in sections 11, 12, 13 of T. 36 S., R. 35 E.. The points are in basalt flows, ash flow, and alluvium (Tba, Twt and Qal). Some of the target pixels in this group are in areas of marsh or playa bed, and may reflect vegetation rather than mineralization.

Group 4 consists of dozens of target pixels spread over sections 2, 3, 6, 7, 8, 11, 14, 15, 16, 17 and 23 of T. 36 S., R. 36 E., and section 33 of T. 35 S., R. 36 E. on the Tule Springs NE and Coyote Meadows quadrangles. Most of these points are in alluvium (Qal) and probably reflect marsh vegetation or salt pan.

Group 5 consists of pixels in section 10, T. 36 S., R. 37 E., on the Coyote Meadows quadrangle. The pixels are in alluvium (Qal), and may reflect marsh vegetation.

Group 6 consists of several groups of points on the Red Mountain and Pole Canyon quadrangles. The first set is in section 34 of T. 37 S., R. 36 E., and is located in alluvium (Qal). The second set is in section 16 T. 38 S., R. 38 E. and coincided with the location of the active Willow Hot springs (46 C) in alluvium (Qal). The third set is located in section 20 T. 38 S., R. 38 E., in Qal, adjacent to a prospect for unknown minerals.

The fourth set is located in section 30 T. 38 S., R. 37 E., in lake sediments (unit Tts) near a group of springs.

Group 7 consists of points in section 34 T. 38 S., R. 38 E., on the Little Whitehorse Creek quadrangle. The site is in ash flow (unit Twt) adjacent to a small rhyolite body (unit Trh).

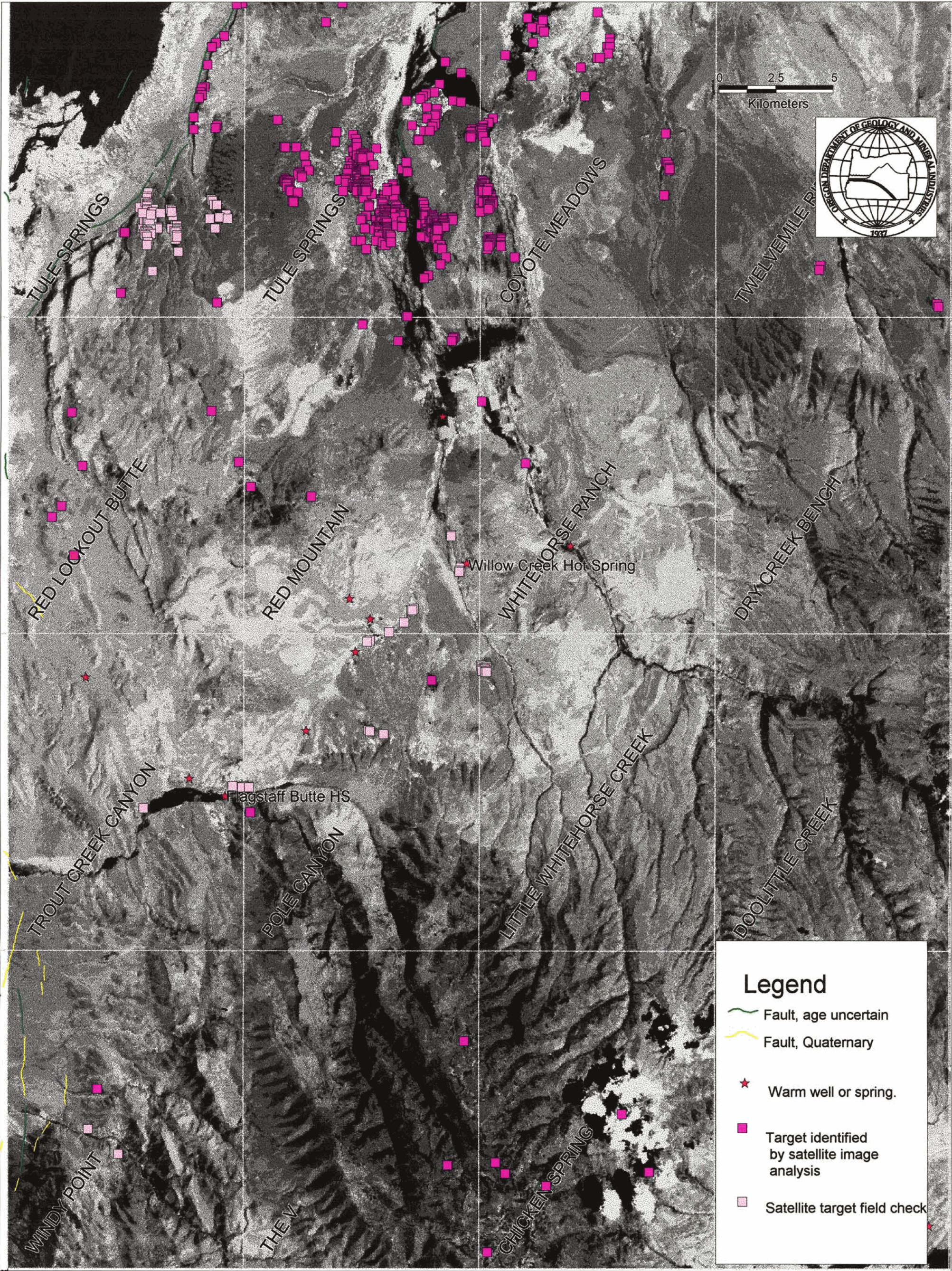
Group 8 is located in section 6 T. 39 S., R. 38 E. on the Pole Canyon quadrangle in lake sediments (unit Tts).

Group 9 is located in section 16 T. 39 S., R. 37 E. on the Trout Creek Canyon quadrangle. The site is in basalt flows (unit Tba) and lake sediments (unit Tts) a few hundred meters northeast of Flagstaff Butte hot springs (53 C).

Group 10 is located in section 26 of T. 40 S., R. 36 E. on the Windy Point quadrangle. The site is in gravels (unit Qtg) in a area of faulting.



Figure 21. Alvord East satellite image





Group 11 consists of scattered points spread across sections 3, 4 and 12 T. 41 S., R. 38 E. on the "The V" and Chicken Springs quadrangles. The sites are in basalt flows (unit Tba).

### **1843 NE**

#### **Alvord Hot Springs**

There was an extensive area of fairly rare spectral characteristics in the marshy fan downslope of Alvord hot springs. These pixels were ignored, because they are almost certainly due to vegetation. There were a few pixels of quite rare characteristics upslope of the springs. These pixels were highly unique in the Band 127, 157, 245 and 247 composites. The entire quarter scene (1843 NE) (Figure 1, 22) for which the search image was developed was searched for those characteristics. The search returned 60,453 pixels out of 8,553,579 (0.706 %), a relatively large number. Upon inspection, it is clear (Figure 22) that the target pixels tend to occur in playa lake environments, particularly around the playa edges, and are thus probably related to vegetation. The year of the image was apparently quite wet, as many of the playas have standing water, and there is extensive snow in the Steens mountain despite the mid-July image date. To further underscore this association, several large areas of target pixels coincide exactly with large irrigated fields. The search characteristics developed from Alvord Hot springs do not appear to be useful.

#### **Mickey Hot Springs**

There were several quite unique pixels adjacent to Mickey Hot Springs. The best signals were in the Band 245 and 347 composites. Searching the surrounding quarter scene (Figure 23) using these characteristics returned 190 out of a total of 8,553,579 pixels (0.0022%). There are several scattered single pixels which may have no significance (Happy Valley, Alvord Hot Springs, Krumbo Reservoir, Flattop Mountain quadrangle). There are also several groups of pixels.

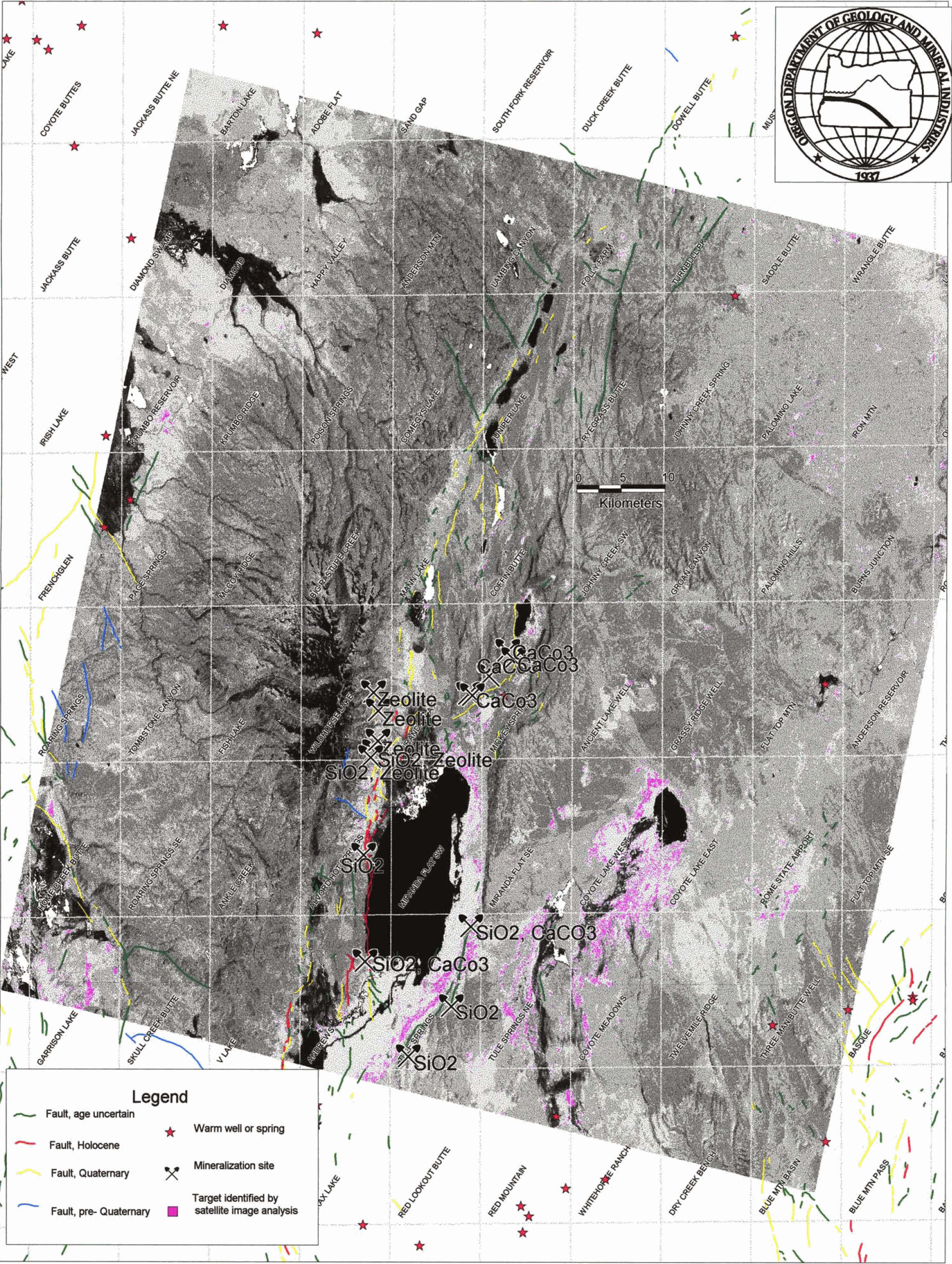
Group 1 includes several pixels located in sections 22, 34 T. 34 S., R. 32 E. and section 4 T. 35 S., R. 32 E. on the Home Creek Butte quadrangle. The sites are located in playa alluvium (unit Qal) and dune sand (unit Qd), and may be associated with vegetation, although the pixels are arranged along the faulted margin of the Catlow valley.

Group 2 occurs in sections 11 and 14, T. 36 S., R. 33 E., on the Andrews quadrangle. The sites are located in playa sediments and dunes (unit Qs) and may be associated with vegetation.

Group 3 occurs on the Alvord Hot Springs quadrangle in section 18 of T. 35 S., R. 34 E.. The site is in alluvium and dune sand (unit Qs), and may be associated with adjacent cultivated fields.

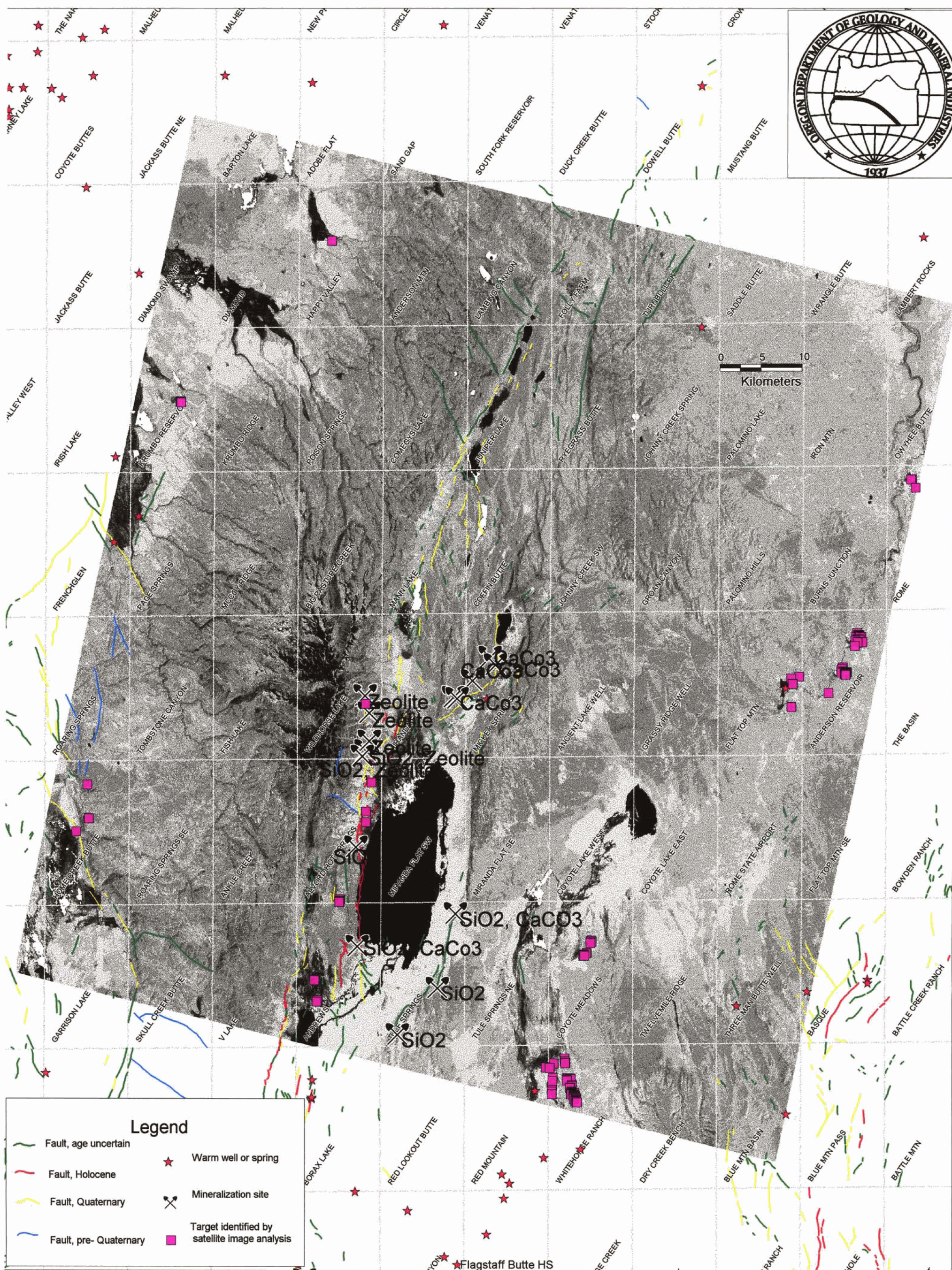


Figure 22. 1843 NE satellite image, Alvord Hot Springs search.





**Figure 23. 1843 NE satellite image, Mickey Hot Springs search.**





The sites occur in areas of lake sediments (unit Ts).

Group 5 occurs in section 34, T. 32 S., R. 40 E., and section 3, 9, and 16, T. 33 S., R. 40 E. on the Anderson Reservoir quadrangle. The sites are associated with basalt flows (unit Tba), alluvium (unit Qal) and terraces (unit Qt).

Group 6 occurs in sections 31 and 32, T. 35 S., R. 37 E. on the Coyote Meadows quadrangle. These sites are in alluvium in an area of seasonal marsh and meadow. Note that there are also many target pixels in this general area from the Easterday hot springs search, though none overlap exactly.

Group 7 occurs in sections 1, 2, 11 and 12, T. 37 S., R. 36 E., and section 18 T. 37 S., R. 37 E. These sites are in alluvium (Qal) and ash flow (unit Twt) but are associated with extensive cultivation.

### **Stink east**

Imagery was examined for the Drewsey area, concentrating on mineralization observed in the field near Drewsey Hot Springs and the newly catalogued hot springs described above (Figure 1, 24). There were some relatively rare pixels near Drewsey Hot Springs, although most occurred in vegetated areas. A few were close to the area of bedrock mineralization and alteration observed in the field. The most promising images were the 134, 137 245, 345 and 357 Band composites. Targets were derived from the combination for the combination of these bands and used to search an image covering roughly the western two-thirds of the Stinkingwater Mountains 1:100,000 scale quadrangle. The search returned 1090 out of 3292264 pixels (.033%). Upon inspection, essentially all of these target pixels were associated with either major stream channels or reservoirs. As such it is apparent that there is no useful alteration signature in the imagery associated with the Drewsey Hot Spring.

### **Field Checks**

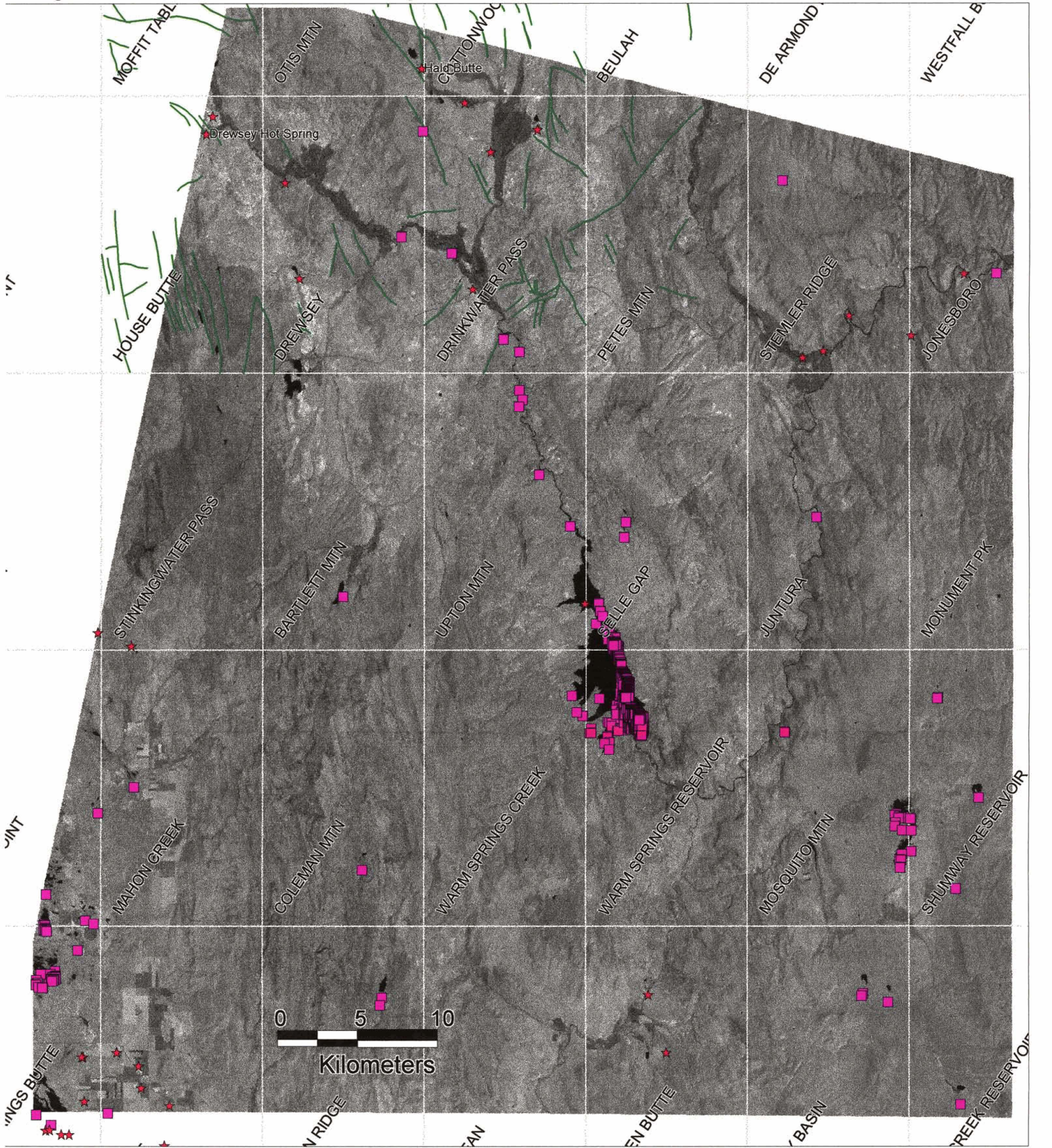
In May of 1996 several of the targets identified on the west half of the Louse Canyon sheet (Figure 20) and the east half of the Alvord Lake sheet (Figure 21) using the Easterday hot springs template were field checked. The results are summarized below.

#### **Target 1**

This target is located on the Rattlesnake Canyon Quadrangle (Figure 20) in the SW quarter of the SE quarter of Section 19, T 35 S. R. 42 E. The target area was located on a steep, partially cliffy slope of welded ash flow tuff (Swisher Mtn) with a lot of exposure, abundant talus and scattered grass and sagebrush. There were no obvious zones of color change or vein and fracture mineralization in the bedrock exposures at the site, but bedrock samples show evidence of silicification and the float contained abundant blocks of highly



Figure 24. Stink East satellite image



Legend

Fault, age uncertain

Warm well or spring

Target identified by satellite image analysis

Satellite target field checked



altered vesicular tuff, stained bright green, silicified with opal fillings in the vesicles. Given the geometry of the slope, it is likely that this site did have a zone of silica mineralization and alteration within a few pixels of the target.

#### Target 2.

This target is located on the Basque quadrangle (Figure 20) in the SE quarter of the NW quarter of section 21. T. 35 S., R. 40 E.. The target area is the floor and walls of a small canyon. The local bedrock is Swisher mountain welded ash-flow tuff, and there is scattered exposure at the target area, with abundant float and some grass. Tuff with pervasive silicification and jasper coatings on fractures was abundant in the float but did not crop out. At this site, there is definitely a zone of silicification within a few pixels of the target.

#### Target 3.

This site is located on the Basque quadrangle (Figure 20) in the NE quarter of the NW quarter of section 8. T. 37 S., R. 42 E. The site is a moderate slope with abundant exposure. Bedrock at the site is platy porphyritic andesite. Chalcedonic quartz veining occurs at the site localized at the intersection of a N60E fault and a buried N70W fault. There is clearly silicification within a few pixels of the target.

#### Target 4.

This target is located on the Blue Mountain Pass quadrangle (Figure 20) in the NE quarter of the NW quarter of Section 17, T. 37 S., R. 42 E.. The site is a moderate slope facing north with rare exposure, some float and thick grass. Bedrock is platy and vesicular welded ash-flow tuff. There is no evidence of mineralization at the site.

#### Target 5.

This target is located on the Blue Mountain Pass quadrangle (Figure 20) in the NE quarter of the SW quarter of Section 21, T. 37 S., R. 42 E.. The site is a small drainage and adjacent moderate slopes, with no exposure, some float and abundant sagebrush and grass. Bedrock is platy and vesicular welded ash-flow tuff. There is no evidence of mineralization at the site.

#### Target 6.

This site is located on the Blue Mountain Basin quadrangle (Figure 20) in the SW quarter of the NE quarter of section 24, T. 37 S., R. 40 E.. The target area consists of a small drainage and adjacent steep slopes with no exposure moderate amounts of float and abundant grass and sagebrush. Bedrock is welded ash-flow tuff. There is no evidence of mineralization at the site.

Target 7.

This site is located on the Red Mountain quadrangle (Figure 21) , in the NE quarter of the NW quarter of section 34 T. 37 S., R. 36 E.. The site is flat, and includes marshy active floodplain of Willow Creek and adjacent older alluvium of distal fanglomerate. The floodplain is heavily vegetated, the older alluvial surface has scattered sagebrush, abundant alkali salt deposits and scattered pebble lag. Aside from the alkali deposits, there is no evidence for mineralization at the site.

Target 8.

This site is located on the Red Mountain quadrangle (Figure 21), in the NE quarter of the NW quarter of section 16 T. 38 S., R. 36 E.. The site includes a small rhyolite body set in older alluvium or distal fanglomerate. The active Willow Creek hot springs (46 C) is within a few pixels of the target. Surficial materials at the target sites is either silicified rhyolite or pebble lag with alkali salts and scattered sagebrush. This site clearly shows evidence for silicification as well as the presence of the active hot spring.

Target 9

This site is located on the Red Mountain quadrangle (Figure 21), in the NE quarter of the NW quarter of section 19 T. 38 S., R. 36 E.. The site is a terrace riser separating older alluvium or distal fanglomerate from the modern alluvial channel. The surface has some exposure, with a fanglomerate pebble lag and scattered sagebrush. The bedrock is diatomite and tuffaceous sediments. The only evidence of mineralization is rare lenticular nodules of chert/flint. There is probably no evidence of silicification or mineralization at this site.

Target 10.

This site is located on the Little Whitehorse creek quadrangle (Figure 21), in the NW quarter of the NW quarter of section 34 T. 38 S., R. 38 E.. The site is a gentle mound with good exposure, some fanglomerate pebble and cobble lag and rare sagebrush. Bedrock at the site is lapilli sandstone, tuffaceous sandstone and siltstone and diatomite. There is no evidence of silicification or mineralization.

Target 11.

This site is located on the Pole Canyon quadrangle (Figure 21), in the SW quarter of the SW quarter of section 6 T. 39 S., R. 38 E.. The site is a moderate north facing slope with some exposure, scattered sagebrush and abundant fanglomerate pebble and cobble lag. The bedrock is lapilli sandstone, tuffaceous sandstone and siltstone and diatomite. There is no evidence of mineralization.

#### Target 12.

This site is located on the Pole Canyon quadrangle (Figure 21) , in the SW quarter of the SE quarter of section 6 T. 39 S., R. 38 E.. The site is a moderate north facing slope with some exposure, scattered sagebrush and abundant fanglomerate pebble and cobble lag. The bedrock is lapilli sandstone, tuffaceous sandstone and siltstone and diatomite. Just south of the target, a small N trending fault cuts the sediment section, and there is some opal in the float along the fault. There is weak evidence for silicification within a few pixels of this target.

#### Target 13

This site is located on the Pole Canyon quadrangle (Figure 21), in the SW quarter of the SW quarter of section 16 T. 39 S., R. 37 E.. The site is a steep south facing slope with abundant exposure, scattered sagebrush and scattered float. The bedrock is rhyolite. At the target there is an extensive alteration zone, involving bleaching of the rhyolite, and mineralization with chalcedony, opal, gypsum, iron oxides and chlorite. There is abundant evidence for mineralization and silicification within a few pixels of this target.

#### Target 14

This site is located on the Trout Creek Canyon quadrangle (Figure 21) in the SW quarter of the NE quarter of section 16, T. 39 S., R. 37 E.. The site is a steep, cliffy south facing slope with abundant exposure, scattered sagebrush and scattered float. The bedrock is rhyolite. The actual target area was too steep to be reached, but showed a clear bleached zone. There is good evidence for mineralization and silicification within a few pixels of this target.

#### Target 15

This site is located on the Trout Creek Canyon quadrangle (Figure 21) in the NE quarter of the NW quarter of section 16, T. 39 S., R. 37 E.. The site is a steep, cliffy south facing slope with abundant exposure, scattered sagebrush and scattered float. The bedrock is rhyolite. The actual target area was too steep to be reached, but showed a clear bleached zone. There is good evidence for mineralization and silicification within a few pixels of this target.

#### Target 16.

This site is located on the Trout Creek Canyon quadrangle (Figure 21) in the SE quarter of the SE quarter of section 13, T. 39 S., R. 36 E.. The site is a moderately steep east facing slope with some exposure, some float and scattered sagebrush and grass. The bedrock is rhyolite. Abundant opal is deposited in fractures and crevices within a blocky zone in the lava flow, and opal fragments to 10 cm thick are common in the float. There is good evidence for silicification within a few pixels of this target.

#### Target 17.

This site is located on the Windy Point (Figure 21) quadrangle in the NE quarter of the SW quarter of section 35, T. 40 S., R. 36 E.. The site is a steep south facing slope with little exposure, abundant float and scattered sagebrush and grass. The bedrock is boulder gravel and pebbly volcanoclastic sandstone. There is no evidence for silicification within a few pixels of this target.

#### Target 18.

This site is located on the Windy Point (Figure 21) quadrangle in the SW quarter of the NW quarter of section 1, T. 41 S., R. 36 E.. The site is a steep northeast-facing slope with abundant exposure and rare sagebrush and grass. The bedrock is a section of basalt flows over 100 m thick dipping about 20 degrees south. High water on Cottonwood creek prevented access to the site, but two reddish zones were observed in the target area in otherwise dark grey basalt. Similar reddish zones in the same section of lavas on the south side of the creek (about .5 km) were interflow zones of bleaching and mineralization with opal, chalcedony and gypsum. There is some evidence for silicification within a few pixels of this target.

#### Target 19

This site is located on the Tule Springs quadrangle (Figure 21) in the SE quarter of the SE quarter of section 9 and the NE quarter of the NE quarter of section 16, T. 36 S. R. 35 E.. The site consists of gentle west facing slopes with some exposure, abundant float and scattered grass and sagebrush. Bedrock at the site consists of tuffaceous sandstone and siltstone with diatomite interbedded with basalt flows. One basalt flow exposed at the site is bleached light grey in color and has pervasive chalcedony mineralization in vesicles and fractures. Opal, chalcedony and petrified wood fragments are abundant in the float. This site has clear evidence of silicification within a few pixels of the target.

#### Target 20

This site is located on the Tule Springs quadrangle (Figure 21) in the SE quarter of section 17 and the NE quarter of section 20 T. 36 S. R. 35 E.. The site consist of a long stretch of west facing moderately steep slope adjacent to a minor drainage. The surface has scattered exposures, extensive basalt colluvial lag and scattered sagebrush and grass. The bedrock is tuffaceous sandstone and siltstone with diatomite, very similar to target 18. There is no evidence for silicification or mineralization near the site.

### Conclusions

It is clear from the above results that Landsat Thematic Mapper data can be used to find some types (generally silicification) of bedrock units under some circumstances. However the largely empirical technique is only successful given



that a suitable mineralized target zone exists on the image. There is no evidence that any mineralization or alteration of Quaternary materials associated with active hot springs can be identified with satellite imagery. This may in part be due to the fact that hot springs in desert environments are typically surrounded by anomalous vegetation which may mask local anomalous mineralization. However, to the extent that active hot springs are associated with silicified bedrock, the technique has promise. The Alvord East image search using the Easterday hot springs model located two active hot springs. Further experimentation with this technique is guardedly recommended, and will only be effective with a considerable investment of field time to check on targets.

## **Conclusions and Recommendations**

From this study we conclude that the use of indirect methods to prospect for undiscovered blind geothermal systems is only moderately useful. The techniques of photogeologic mapping of faults coupled with reconnaissance field investigation to look for mineralization only turned up one likely target out of 11 areas studied. Similarly the analysis of satellite imagery did not identify any likely targets, although resources for field checking satellite imagery targets were limited. At best these techniques can eliminate some areas (Guano, Catlow) and prioritize those which might be targets for further exploration (Owhyee Uplands, Antelope Valley, Drewsey and Christmas Lake-Summer Lake). The indirect methods are likely to be most useful when used to target gradient hole drilling. Without the confirmation provided by actual gradient measurements, the indirect methods can only serve as crude guides.

Of all the areas studied, the ~~two~~<sup>three</sup> that we believe have the greatest potential for significant undiscovered resources are The Christmas Lake-Summer Lake area, the Antelope Valley area and the Drewsey area. Although there is very little data in each of these areas, all of it points to a potential resource. The oxygen isotope study indicates that a relatively hot system may have been active at Egli Rim during the Holocene, and the area has unusually high fracture permeability. Ground water studies (Hampton, 1964) suggest that there is considerable flow from the Christmas Lake basin south to the Summer Lake basin, which may mask underlying geothermal systems. Similarly the Drewsey and Antelope valley areas may both have some masking of geothermal waters by flow of abundant shallow cold water from adjacent highlands. In all three of these areas there are not enough heat flow data to establish the presence or absence of a resource. We recommend the future investigations should focus on gradient hole drilling in these three areas.

## References

- Allison, I. (1982) Geology of pluvial Lake Chewaucan, Lake County, Oregon. Oregon State University Press, Corvallis.
- Blackwell, D. D., 1995 Geothermal Gradients in Oregon, 1985-1994: Oregon Department of Geology and Mineral Industries Open-File Report O-95-3, 132 pp.
- Blackwell, D.; Hull, D.A.; Bowen, R.G.; Steele, J.L. 1978. Heat flow of Oregon: Oregon Department of Geology and Mineral Industries, Special paper 4, 42 pp.
- Brown, D.E.; Peterson, N.V.; McLean, G.D. 1980. Preliminary geology and geothermal resource potential of the Lakeview area, Oregon. DOGAMI Report O-80-9.
- Evans, J.G. 1990. Geology and Mineral Resources Map of the South Mountain Quadrangle, Malheur County, Oregon. Oregon Department of Geology and Mineral Industries Geologic Map Series GMS-67.
- Hampton, E.R., 1964, Geologic factors that control the occurrence and availability of groundwater in the Fort Rock Basin, Lake County, Oregon: U.S. Geological Survey Prof. Paper 383-B, p. B1-B29.
- Hemphill-Haley, M.A.; Page, W.D.; Burke, R.; Carver, G.A. 1989. Holocene activity of the Alvord Fault, Steens Mountain, southeastern Oregon (report) 38pp. Woodward-Clyde Consultants, Oakland, California.
- Jellinek, A. M., Madin, I.P., and Langridge, R., 1996, Field and stable isotope indicators of geothermal resource potential, central Lake County, Oregon. Oregon Geology, V. 58, no. 1, p 3-9.
- Lawrence, R.D. 1978. Strike-slip faulting terminates the Basin and Range in Oregon. Geological Society of America Bulletin 87: 846-850.
- McLeod, N.S.; Walker, G.W.; McKee, E.H. 1975. Geothermal significance of eastward increase in age of upper Cenozoic rhyolite domes in southeastern Oregon. U.S. Geological Survey Open-file Report 75-348.
- Peterson, N.V.; Brown, D.E. 1980. Preliminary geology and geothermal resource potential of the Alvord Desert area, Oregon. DOGAMI report O-80-10.
- Peterson, N.V., Priest, G.R., Black, G.L., Brown, D.E., Woller, N.M., Blackwell, D.D., Steele, J.L., and Justus, D., 1982. Geothermal Resources of Oregon. DOGAMI/NOAA. 1:500,000 scale Map.
- Pezzopane, S.K. 1993. Active faults and earthquake ground motions in Oregon. Ph.D. Dissertation, University of Oregon, 208pp.
- Stafford, H.S. 1935. A regional geomorphic study of the Guano Valley. MA thesis, University of Oregon
- Walker, G.W., and MacLeod, N.S., 1991. Geologic map of Oregon 1:500,000. U.S. Geological Survey, Washington, D.C.
- Walker, G.W.; Repenning, C.A. 1966. Reconnaissance geologic map of the west half of the Jordan Valley quadrangle, Malheur County, Oregon, scale 1:250,000. U.S. Geological Survey Map I-457.

**Appendix 1.**  
**Oxygen Isotope Study**



## Field and stable isotope indicators of geothermal resource potential, central Lake County, Oregon

by A. Mark Jellinek, *Research School of Earth Sciences, The Australian National University, Canberra*; Ian P. Madin, *Oregon Department of Geology and Mineral Industries*; and Robert Langridge, *University of Oregon*

### ABSTRACT

The geothermal resource potential in central Lake County, Oregon, has been known for some time on the basis of active hot springs and hot wells in the Summer Lake Known Geothermal Resource Area, scattered warm springs at the north end of Summer Lake and on the east shore of Lake Abert, and a single published borehole heat-flow measurement at Paisley. We report field and stable isotopic evidence for Quaternary hot springs at the north end of Lake Abert and in the Picture Rock Pass area that indicate the presence of recently active paleogeothermal systems. At the north end of Lake Abert, tufa mounds and travertine vein fillings are possibly associated with a zone of intersecting northeast- and northwest-trending faults. The tufa mounds occur in a narrow elevation range, a feature that suggests their deposition was controlled by the Pleistocene lake level. At Picture Rock Pass, travertine and silica sinter mineralization occurs in fractures, joints, and cavities in basalt bedrock, in Pliocene or Quaternary channel gravels, and in Holocene colluvium associated with the Egli Rim escarpment and an adjacent network of closely spaced northeast- and northwest-trending faults. The  $\delta^{18}\text{O}$  (SMOW) and  $\delta^{13}\text{C}$  (PDB) data for samples of travertine from the study areas range from 16.1 to 17.4 per mil and  $-6.8$  to  $-10.7$  per mil, respectively, at Picture Rock Pass and from 24.0 to 28.9 per mil and 1.4 to 4.5 per mil, respectively, at Lake Abert. These data are similar to analogous data from geothermal areas in New Zealand, central Italy, western Germany, southwestern Colorado, and Yellowstone in Wyoming. Surface precipitation temperatures for samples of sinter and travertine from the Picture Rock Pass area are determined with equilibrium oxygen-isotopic thermometry to be  $39^{\circ}$ – $70^{\circ}\text{C}$  and  $30^{\circ}$ – $49^{\circ}\text{C}$ , respectively, and are geologically reasonable. The precipitation temperatures for samples of Picture Rock Pass sinter combined with temperature-dependent solubility curves of Rimstidt and Cole (1983) for amorphous silica and quartz indicate geothermal reservoir temperatures of  $145^{\circ}$ – $205^{\circ}\text{C}$  and suggest that the Picture Rock Pass sinter was precipitated from a hot-water system. The results of the field and stable isotopic studies indicate a significant geothermal resource potential at both sites.

### INTRODUCTION

This study is part of a program of the Oregon Department of Geology and Mineral Industries (DOGAMI) to prospect for geothermal resources in southeastern Oregon

by looking for geologic evidence of late Quaternary hot spring activity. The program began in 1992 and is funded by the Bonneville Power Administration, the U.S. Department of Energy, and Portland General Electric Company.

Most of the Known Geothermal Resource Areas (KGRAs) in southeast Oregon (Alvord, Crump Geyser, Lakeview, Summer Lake, and Klamath Falls) are spatially associated with major Basin and Range faults (Oregon Department of Geology and Mineral Industries/NOAA, 1982). All of these KGRAs have natural hot springs, and the Alvord KGRA (Hemphill-Haley and others, 1989), Summer Lake KGRA (Pezzopane, 1993), and Klamath Falls KGRA (Sherrod and Pickthorn, 1992) show evidence of Holocene faulting. The program's aim is to use the association of faulting and hot springs to locate new areas of geothermal potential by locating evidence for geologically young but currently inactive hot springs associated with Neogene faulting in southeast Oregon. We report the results of preliminary field and stable isotopic studies from two sites in central Lake County, Oregon (Figure 1). The two areas, Picture Rock Pass and Sawed Horn (at the north end of Lake Abert), were selected for detailed field investigation on the basis of complex and closely spaced faulting observed with photogeologic mapping and in the field. Neither site has a known hot spring or hot well, but both sites showed evidence of late Quaternary or Holocene hot springs in the form of travertine and sinter mineralization precipitated into Miocene basalt bedrock, Pliocene or Quaternary channel gravels, and Holocene colluvium. Both sites were mapped at 1:24,000 scale, and the travertine and sinter were sampled.

Stable isotopic data are presented for samples of travertine and sinter collected from the Picture Rock Pass area and for samples of travertine collected from the Sawed Horn area. Oxygen and carbon isotopic data for the Lake Abert and Picture Rock Pass travertine are compared with similar data from travertine of central Italy, southwest Colorado, western Germany, Yellowstone National Park, and the Broadlands geothermal field in New Zealand. Additionally, surface saturation temperatures for fluids precipitating travertine and surface saturation and geothermal reservoir temperatures for fluids precipitating sinter from the Picture Rock Pass area are determined with oxygen isotope thermometry on the basis of temperature-dependent equilibrium quartz-water and calcite-water isotope fractionations.

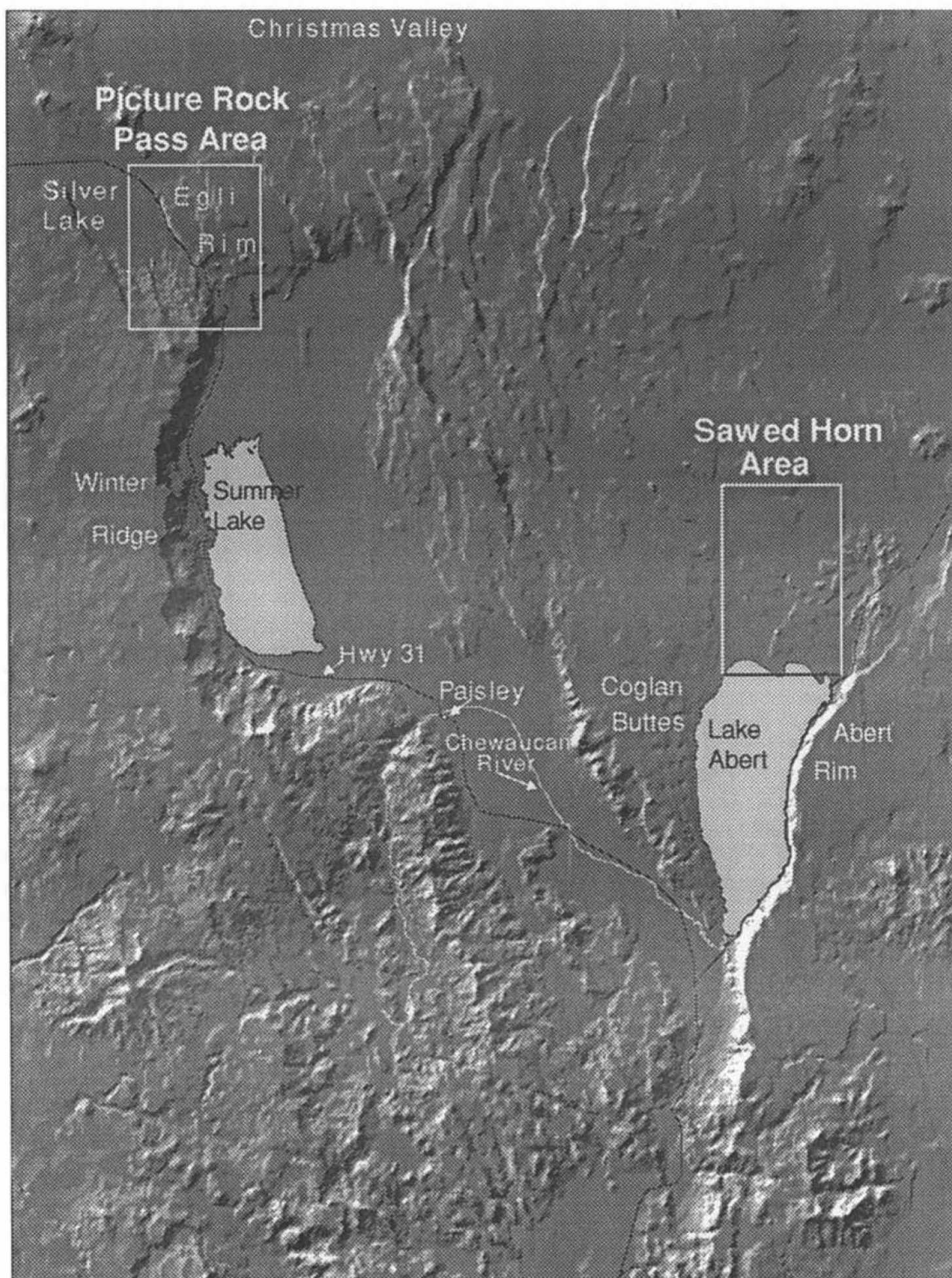


*Figure 1. Shaded-relief map of central Lake County showing study areas.*



## PICTURE ROCK PASS

The Picture Rock Pass study area is located on the Egli Rim 7½-minute quadrangle astride Highway 31 between two major Basin and Range basins, Silver Lake to the north and Summer Lake to the south (Figure 1). The bedrock is predominantly Miocene basalt (Hampton, 1964; Walker and others, 1967; Travis, 1977; Walker and McLeod, 1991). Fiebelkorn and others (1983) report a K-Ar age of  $6.9 \pm 0.9$  Ma for basalt at Picture Rock Pass. Bedrock in the study area is cut by numerous, commonly intersecting, northeast- and northwest-trending faults (Figure 2). Paleochannels follow many of the grabens developed between the intersecting faults, and Pliocene or Quaternary cobble gravel deposits fill the channels. Where the channels are cut by intersecting faults, numerous small Pliocene or Quaternary playa lakes have formed. Quaternary lacustrine deposits fill the Silver Lake basin west of the Egli Rim, and Holocene colluvium mantles the escarpment of the Egli Rim.

Samples of sinter and travertine were collected from the cobble gravel; colluvium; and cavities, fractures, and joints

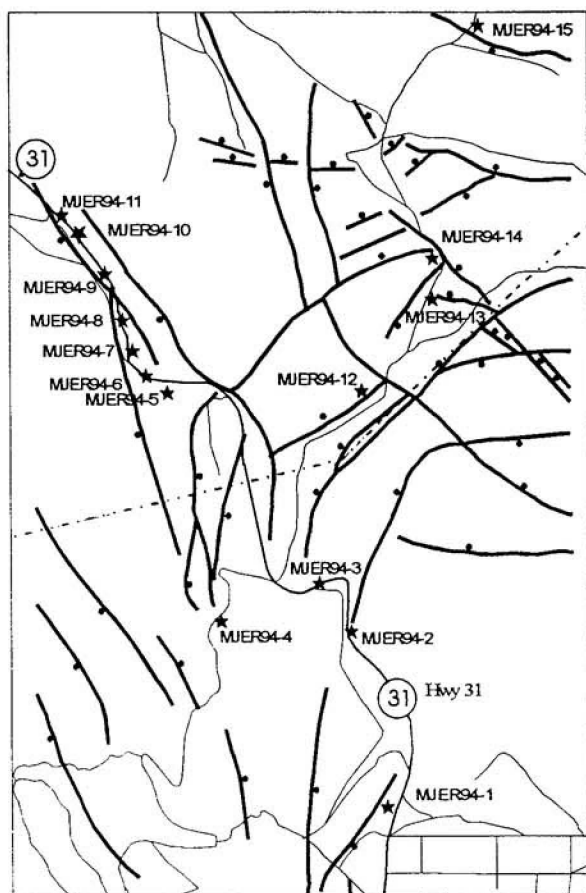


Figure 2. Sketch map of the Picture Rock Pass area, Egli Rim quadrangle. Heavy lines are faults, with ball on down-thrown side. Fine lines are unimproved roads; dot-and-dash line is a transmission line. Stars show sample locations.

in basalt flows along the Egli Rim (Figure 1). The best exposures of sinter and travertine occur in road-cuts along Highway 31 and the other unimproved roads in the area. The proximity of these exposures to regional faults and fault intersections suggests that the movement of associated geothermal fluids was strongly fault controlled.

In most sampled exposures, travertine is a soft, white- to cream-colored rind on typically vitreous, honey-colored to yellow or tan, hard to friable siliceous sinter. The stratigraphic position of travertine on top of sinter indicates that the two phases were probably not syndepositional. In exposures of altered colluvium, sinter is friable, occurs as meter-scale layers or paleoterraces, and can contain internal, centimeter-scale layers that are fine grained to conglomeratic. Packages of centimeter-scale layers can include rhythmic interbeds of sinter and travertine. The pebbles constituting conglomeratic layers are generally well rounded and attributed to the host sediment. The sedimentary appearance of these exposures is similar, for example, to that described for the Beowawe, Nevada, sinter deposit (Rimstidt and Cole, 1983).

In exposures of altered and mineralized cobble gravels, boulders, and basalt flows, sinter occurs as a hard, smooth or rough glaze up to 2 cm thick that is also typically coated by rinds of travertine. Minor brecciation is common, particularly in exposures along Highway 31. Mineralized zones hosted by cobble gravel are typically massive, up to 7 m thick, and stratigraphically confined to gravel horizons of high permeability. Alteration zones in basalt flows are rectangular to prolate and up to 10 m high and can have aspect ratios of 60:1. Mineralization is typically confined to single flows within flow packages, which suggests that certain flows exhibit greater fracture permeability than others.

## SAWED HORN

Lake Abert occupies a Basin and Range graben bounded by the Abert Rim to the east and Cogan Buttes to the west (Figure 1). The Sawed Horn study area is an area of faulted bedrock at the north end of the graben and is on the Sawed Horn and Lake Abert North 7½-minute quadrangles. The bedrock consists of Miocene basalt flows overlain by the Miocene Rattlesnake Ash-flow Tuff (Walker and MacLeod, 1991). Quaternary beach, dune, and lacustrine deposits overlie the bedrock along the north shore of the lake. Numerous well-defined northwest- and northeast-trending faults cut the bedrock units (Figure 3). Several travertine mounds overlie the Quaternary deposits at an elevation of about 4,390 ft and may be associated with the projections of faults beneath the alluvium. Travertine also occurs as vein fillings in joints and fractures in the basalt bedrock.

The mounds are oblate to mushroom-shaped, 1–3 m high, and constructed of weakly bedded to massive, spongy, and exceedingly porous carbonate material or tufa (Turi, 1986). The relative proportions of calcite and aragonite are not known. Several mounds have rounded pebbles and cobbles of the host sediment entrained in their bases. Their occurrences at similar elevations suggest a rela-



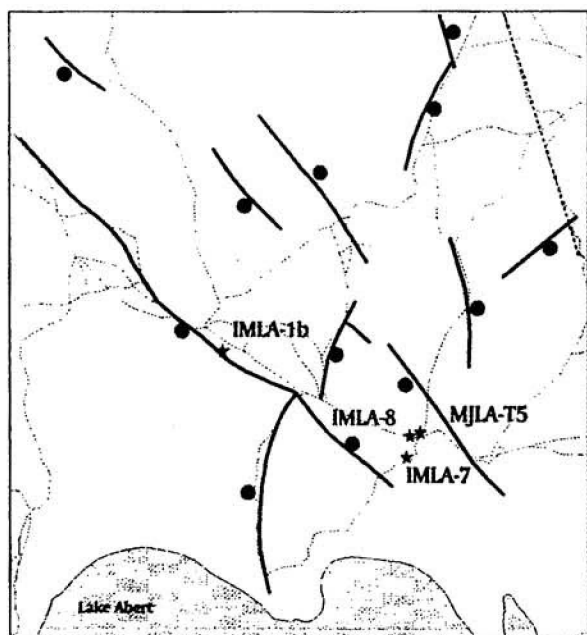


Figure 3. Sketch map of the Lake Abert North and Sawed Horn quadrangles. Heavy lines are faults, with ball on downthrown side. Dashed lines are unimproved roads. Dot-and-dash line is a transmission line. Stars show sample locations.

tionship to paleo-lake level. Samples were collected from tufa mounds and travertine vein fillings in the Sawed Horn area, and one tufa mound was sampled (COGBUT-1) on the shore of Lake Abert, several kilometers southwest of the study area.

#### OXYGEN AND CARBON ISOTOPES AND THERMOMETRY

Samples of travertine and sinter were collected and analyzed for stable isotopic characterization and comparison with other geothermal areas around the world. Oxygen isotope data are also used with appropriate equilibrium fractionation equations to determine travertine and amorphous silica surface saturation temperatures for the geothermal fluids of Picture Rock Pass in order to evaluate fluid reservoir temperatures (Fournier and Rowe, 1966; Rimstidt and Barnes, 1980; Rimstidt and Cole, 1983). Temperatures determined in this way are generally in good agreement with measured precipitation temperatures (Clayton and others, 1968; Friedman, 1970). The methods of McCrea (1950) and Borthwick and Harmon (1982) were employed to determine  $^{18}\text{O}/^{16}\text{O}$  ratios for siliceous sinter and  $^{18}\text{O}/^{16}\text{O}$  and  $^{13}\text{C}/^{12}\text{C}$  ratios for travertine. The analyses were performed at the Stable Isotope Laboratory at Washington State University. The  $^{18}\text{O}/^{16}\text{O}$  ratios are reported relative to the standard mean ocean water standard (SMOW) and the  $^{13}\text{C}/^{12}\text{C}$  ratios relative to the PDB (Peedee belemnite) standard as  $\delta^{18}\text{O}$  and  $\delta^{13}\text{C}$  values in per mil, respectively.

The  $\delta^{18}\text{O}$  and  $\delta^{13}\text{C}$  data are tabulated with comparative analyses from other studies in Table 1. The  $\delta^{18}\text{O}$  values are not included for all of the comparative studies because global comparison of  $\delta^{18}\text{O}$  values for hydrothermal travertine and sinter is complicated by latitude-controlled variations in the  $\delta^{18}\text{O}$  values for meteoric water (Taylor, 1974), from which the two phases acquire most of their oxygen. Shallow geothermal fluids are composed of nearly purely meteoric water (Truesdell and Fournier, 1976; Truesdell and others, 1977; Taylor, 1979). The  $\delta^{18}\text{O}$  data for travertine of central Italy and southwest Colorado are included because they are from study areas of similar latitude to south-central Oregon. Analogous  $\delta^{18}\text{O}$  values for sinter are currently unavailable.

The  $\delta^{18}\text{O}$  data for Picture Rock Pass sinter vary from 17.5 to 21.5 per mil. The  $\delta^{18}\text{O}$  and  $\delta^{13}\text{C}$  data for travertine range from 16.1 to 17.7 per mil and -6.8 to -10.7 per mil, respectively. The  $\delta^{18}\text{O}$  values are similar to those reported by Chafetz and others (1991) for travertine deposited from a warm spring in southwest Colorado and are substantially lighter than values given by Turi (1986) for travertine of central Italy. The  $\delta^{13}\text{C}$  values are analogous to data of Savelli and Wedepohl (1969) for travertine of the Westerhof, Göttingen, and Iburg areas of western Germany and to data of Blattner (1975) for travertine of the Broadlands geothermal field, New Zealand. The  $\delta^{18}\text{O}$  values for samples of Lake Abert tufa mounds vary from 24.0 to 28.9 per mil and are similar to values recorded by Turi (1986) for travertine of central Italy. The  $\delta^{13}\text{C}$  data range from 1.4 to 4.5 per mil and are analogous to data reported by Friedman (1970) for samples of travertine from New Highland Terrace, Mammoth Hot Springs, Yellowstone National Park, and also similar to data of Turi (1986). These  $\delta^{18}\text{O}$  and  $\delta^{13}\text{C}$  values are considerably heavier than those of Picture Rock Pass samples.

Precipitation temperatures are determined for sinter and travertine samples from Picture Rock Pass with the assumption that the geothermal fluids and precipitates were in stable isotopic equilibrium at the time of their deposition (Bottinga and Javoy, 1973; O'Neil, 1986; Clayton and others, 1989). We evaluated the equilibrium fractionation temperatures for sinter using the quartz-water fractionation equation of Sharp and Kirschner (1994):

$$\delta^{18}\text{O}_{\text{qtz}} - \delta^{18}\text{O}_{\text{H}_2\text{O}} = 3.65(10^6/T^2) - 2.9 = 10001n\alpha,$$

where  $T$  is absolute temperature and  $\alpha$  is the fractionation factor. We determined similar temperatures for travertine by combining the quartz-calcite and quartz-water fractionation equations of Clayton and others (1989) and Sharp and Kirschner (1994) into a calcite-water fractionation equation:

$$\delta^{18}\text{O}_{\text{Cc}} - \delta^{18}\text{O}_{\text{H}_2\text{O}} = 3.27(10^6/T^2) - 2.95 = 10001n\alpha.$$

We calculated the  $\delta^{18}\text{O}_{\text{H}_2\text{O}}$  values for meteoric water of south-central Oregon, which are taken to be equivalent to geothermal fluid values, using the meteoric water line and

Table 1. Stable isotope data from this and comparative studies along with calculated precipitation temperatures of samples of travertine and sinter from Picture Rock Pass. Values in per mil

	Sample number	$\delta^{18}\text{O}$	$\delta^{13}\text{C}$	$T_p (-112.5)^*$	$T_p (-13.75)^*$	$T_p (-15)^*$
<b>Picture Rock Pass</b>						
<b>Sinter</b>	MJER 94-2	17.5	—	60.0	53.8	48.0
	MJER 94-3	21.5	—	41.4	36.2	31.3
	MJER 94-8	18.7	—	54.0	48.1	42.6
	MJER 94-4	21.5	—	41.3	36.1	31.1
	MJER 94-10	19.7	—	49.1	43.5	38.2
	MJER 94-12	15.8	—	68.9	62.3	56.0
<b>Travertine</b>	MJER 94-9	17.3	-8.4	42.6	36.7	31.2
	MJER 94-11	17.7	-7.7	40.9	35.1	29.7
	MJER 94-1	16.8	-10.7	45.2	39.3	33.6
	MJER 94-7	16.1	-6.8	48.9	42.7	36.9
	MJER 94-5	17.0	-8.8	44.4	38.4	32.8
	MJER 94-13	17.4	-6.8	42.5	36.6	31.2
<b>Sawed Horn</b>						
<b>Travertine</b>	IMLA-7	24.9	1.8	—	—	—
	COGBUT-1	24.0	1.4	—	—	—
	IMLA-8	24.8	1.3	—	—	—
	IMLA-1b	28.9	4.5	—	—	—
	MJLA-5	24.8	1.5	—	—	—
<b>Comparative studies</b>						
	Chafetz and others (1991)	16.74 to 16.95	-2.89 to -2.70	33.21	—	—
	Blattner (1975)	—	-5.4 to -10.2	—	—	—
	Friedman (1970)	—	1.7 to 4.3	73 to 30.5	—	—
	Turi (1986)	16 to 26	-4 to 8	—	—	—
	Savelli and Wedepohl (1969)	—	-10 to -7	—	—	—

\*  $T_p (x)$  is the calculated precipitation temperature in degrees Celsius for the phase in equilibrium with meteoric water that has a  $\delta^{18}\text{O}$  value of  $x$ .

$\delta\text{D}$  values reported by Taylor (1974) for meteoric surface waters of south-central Oregon and northern Nevada. The  $\delta^{18}\text{O}_{\text{H}_2\text{O}}$  values used in this study are  $-13.8 \pm 1.3$  per mil and assume negligible  $^{18}\text{O}$ -shifting to higher values as a result of the interaction of hot geothermal waters with their host rocks.

Calculated surface saturation temperatures for fluids precipitating samples of Picture Rock Pass sinter and travertine are tabulated in Table 1. The  $\delta^{18}\text{O}$  values for samples of Lake Abert tufa were too heavy to allow geologically reasonable temperatures to be calculated with equilibrium isotope thermometry—a feature that may reflect significant evaporation occurring as the tufa was precipitated. For Picture Rock Pass samples, the ranges of precipitation temperatures predicted are  $30^\circ$ – $49^\circ\text{C}$  for travertine and  $31^\circ$ – $70^\circ\text{C}$

for sinter and are geologically reasonable. Travertine and sinter are typically deposited by waters cooling through  $75^\circ$ – $25^\circ\text{C}$  and  $100^\circ$ – $50^\circ\text{C}$ , respectively (Friedman, 1970; Rimstidt and Cole, 1983). The consistent stratigraphic position of travertine on top of sinter in outcrops of altered alluvium, colluvium, and basalt suggests that the precipitation of these two phases was sequential and may, in part, reflect changes in the thermal histories of the geothermal fluids. Temperatures predicted for two travertine/sinter sample pairs, ER94-1/ER94-2 and ER94-9/ER94-10, suggest that the precipitation of travertine after sinter correlates with cooling of the geothermal fluids. Finally, assuming that the surface fluids were saturated in amorphous silica, the reservoir fluid equilibrated with quartz, and there was no subsurface boiling, one can use Figure 1 of Rimstidt

and Cole (1983) to evaluate reservoir fluid temperatures on the basis of the different temperature-dependent solubilities of amorphous silica and quartz (see also Truesdell and Fournier, 1976; Rimstidt and Barnes, 1980). Sinter precipitated from fluids saturated in amorphous silica at 30°–50°C indicates geothermal reservoir temperatures of 145°–205°C.

## CONCLUSION

The results of the preliminary stable isotope study support three conclusions. The first is that  $\delta^{18}\text{O}$  and  $\delta^{13}\text{C}$  data for samples of travertine from Picture Rock Pass and Lake Abert tufa mounds are similar to analogous data for travertine from other geothermal areas around the world. Second, precipitation temperatures for sinter and travertine determined with oxygen isotope thermometry of 31°–70°C and 30°–49°C, respectively, are geologically reasonable. Last, precipitation temperatures for sinter combined with the temperature-dependent solubility curves of Rimstidt and Cole (1983) for amorphous silica and quartz indicate geothermal reservoir temperatures of 145°–205°C. This assessment assumes that the surface fluids were saturated with respect to amorphous silica, that the reservoir fluid equilibrated with quartz, and that there was no subsurface boiling.

These results also suggest that hot springs systems were active at the north end of Lake Abert during the late Quaternary and at Picture Rock Pass during the late Quaternary and Holocene. The combination of geologically recent hot spring activity and extensive faulting in both of these areas indicates that they have significant geothermal resource potential. Further work, including local heat flow measurements, is warranted to better evaluate the resource potential of both areas.

## ACKNOWLEDGMENTS

We owe thanks to Peter Larson for review of the stable isotope portion of this paper and Mark Ferns and Gerald Black for review of the geologic portion of the paper.

## REFERENCES CITED

- Blattner, P., 1975, Oxygen isotopic compositions of fissure-grown quartz, adularia, and calcite from Broadlands geothermal field, New Zealand, with an appendix on quartz-K-feldspar-calcite-muscovite oxygen isotope geothermometers: *American Journal of Science*, v. 275, p. 785–800.
- Borthwick, J., and Harmon, R.S., 1982, A note regarding CIF3 as an alternative to BrF3 for oxygen isotope analysis: *Geochimica et Cosmochimica Acta*, no. 46, p. 1665–1668.
- Bottinga, Y., and Javoy, M., 1973, Comments on stable isotope geothermometry: *Earth and Planetary Sciences Letters*, no. 20, p. 250–265.
- Chafetz, H.S., Rush, P.F., and Utech, N.M., 1991, Microenvironmental controls on mineralogy and habit of  $\text{CaCO}_3$  precipitates: An example from an active travertine system: *Sedimentology*, v. 38, p. 107–126.
- Clayton, R.N., Goldsmith, J.R., and Mayeda T.K., 1989, Oxygen isotope fractionation in quartz, albite, anorthite, and calcite: *Geochimica et Cosmochimica Acta*, v. 53, p. 725–733.
- Clayton, R.N., Muffler, L.J.P., and White, D.E., 1968, Oxygen isotope study of calcite and silicates of the River Ranch No. 1 well, Salton Sea geothermal field, California: *American Journal of Science*, v. 266, p. 968–979.
- Fiebelkorn, R.B., Walker, G.W., MacLeod, N.S., McKee, E.H., and Smith, J.G., 1983, Index to K-Ar age determinations for the State of Oregon: *Isochron/West* 37, p. 3–60.
- Fournier, R.O., and Rowe, J.J., 1966, Estimation of underground temperatures from the silica content of water from hot springs and wet-steam wells: *American Journal of Science*, v. 264, p. 685–697.
- Friedman, I., 1970, Some investigations of the deposition of travertine from hot springs. 1—The isotopic chemistry of a travertine-depositing spring: *Geochimica et Cosmochimica Acta*, v. 34, p. 1303–1315.
- Hampton, E.R., 1964, Geologic factors that control the occurrence and availability of ground water in the Fort Rock Basin, Lake County, Oregon: U.S. Geological Survey Professional Paper 383-B, 29 p.
- Hemphill-Haley, M.A., Page, W.D., Burke, R., and Carver, G.A., 1989, Holocene activity of the Alvord Fault, Steens Mountain, southeastern Oregon: Unpublished report, Woodward-Clyde Consultants, Oakland, Calif., 38 p.
- McCrea, J.N., 1950, On isotopic chemistry of carbonates and the paleotemperature scale: *Journal of Chemical Physics*, v. 18, p. 849–857.
- O'Neil, J.R., 1986, Theoretical and experimental aspects of isotopic fractionation, in Valley, J.W., Taylor, H.P., and O'Neil, J.R., Stable isotopes in high temperature geological processes (Reviews in Mineralogy, v. 16): Washington D.C., Mineralogical Society of America.
- Oregon Department of Geology and Mineral Industries/NOAA, 1982, Geothermal resources of Oregon, 1982: National Oceanic and Atmospheric Administration (for U.S. Department of Energy), 1 map, scale 1:500,000.
- Pezzopane, S.K., 1993, Active faults and earthquake ground motions in Oregon: Eugene, Oreg., University of Oregon doctoral dissertation, 208 p.
- Rimstidt, J.D., and Barnes, H.L., 1980, The kinetics of silica-water reactions: *Geochimica et Cosmochimica Acta*, v. 44, p. 1683–1699.
- Rimstidt, J.D., and Cole, D.R., 1983, Geothermal mineralization I: The mechanism of formation of the Beowawe, Nevada, siliceous sinter deposit: *American Journal of Science*, v. 283, p. 861–875.
- Savelli, C., and Wedepohl, K.H., 1969, Geochemische Untersuchungen an Sinterkalken (Travertinen): *Beiträge zur Mineralogie und Petrologie (Contributions to Mineralogy and Petrology)*, v. 21, p. 238–256.
- Sharp, Z.D., and Kirschner, D.L., 1994, Quartz-calcite oxygen isotope thermometry: A calibration based on natural isotopic variations: *Geochimica et Cosmochimica Acta*, v. 58, p. 4491–4501.
- Sherrod, D.R., and Pickthorn, L.G., 1992, Geologic map of the west half of the Klamath Falls 1° by 2° quadrangle, south-central Oregon: U.S. Geological Survey Miscellaneous Investigations Map I-2182, scale 1:250,000.
- Taylor, H.P., 1974, The application of oxygen and hydrogen isotope studies to problems of hydrothermal alterations and ore deposition: *Economic Geology*, v. 69, p. 843–883.



- , 1979, Oxygen and hydrogen isotope relationships in hydrothermal mineral deposits, in Barnes, H.L., ed., *Geochemistry of hydrothermal ore deposits*, 2d ed.: New York, John Wiley, p. 236–277.
- Travis, P.L., 1977, *Geology of the area near the north end of Summer Lake, Lake County, Oregon*: Eugene, Oreg., University of Oregon master's thesis, 95 p.
- Truesdell, A.H., and Fournier, R.O., 1976, Conditions in the deeper parts of the hot spring systems of Yellowstone National Park, Wyoming: U.S. Geological Survey Open-File Report 76–428, 29 p.
- Truesdell, A.H., Nathenson, M., and Rye, R.O., 1977, The effect of subsurface boiling and dilution on the isotopic compositions of Yellowstone thermal waters: *Journal of Geophysical Research*, v. 82, p. 3694–3704.
- Turi, B., 1986, Stable isotope geochemistry of travertines, in Fritz, P., and Fontes, J.C., eds., *The terrestrial environment*: Amsterdam, Elsevier.
- Walker, G.W., and MacLeod, N.S., 1991, *Geologic map of Oregon*: U.S. Geological Survey Special Geologic Map, 1:500,000.
- Walker, G.W., Peterson, N.V., and Greene, R.C., 1967, Reconnaissance geologic map of the east half of the Crescent quadrangle, Lake, Deschutes, and Crook Counties, Oregon: U.S. Geological Survey Miscellaneous Investigations Map I-493, 1:250,000. □

(Continued from page 2)

## Earthquake IQ test answers

1. **Question:** What is generally considered to be a "major" earthquake?  
**Answer:** b — Magnitude (M) 7. However, smaller magnitude earthquakes can be very damaging. Remember, the M 5.6 earthquake on March 1993 at Scotts Mills ("Spring Break Quake") caused minor damage (about \$30 million). The *intensity* scale (expressed in Roman numerals) describes the effects people experienced ("felt effects") from an earthquake and can be associated with damage levels.
2. **Question:** When will the next big earthquake be?  
**Answer:** b — No one knows. No one can reliably predict "when, where, and how big" the next earthquake will be.
3. **Question:** What do you do *during* an earthquake?  
**Answer:** d — It really depends on where you are. (1) If you are indoors, *duck* or drop down to the floor. Take *cover* under a sturdy desk, table, or other furniture. *Hold* on to it and be prepared to move with it. Hold the position until the ground stops shaking and it is safe to move. Stay clear of windows, fireplaces, wood stoves, and heavy furniture or appliances. Stay inside. Outside, you may be injured by falling glass or building parts. If you are in a crowded area, take cover and stay where you are. Stay calm and encourage others to do likewise. (2) If you are outside, get into the open, away from buildings, power lines, and trees. (3) If you are driving, stop if it is safe, but stay inside your car. Stay away from bridges, overpasses, and tunnels. Move your car as far out of the normal traffic pattern as possible. Avoid stopping under trees, light posts, power lines, or signs if possible. (4) If you are in a mountainous area, or near unstable slopes or cliffs, be alert for falling rock and other debris that could be loosened by the earthquake.
4. **Question:** What do you do immediately *after* an earthquake?  
**Answer:** e — Both c and d. Check for injuries, hazards (fire, gas leaks, spills, etc.), clean up, expect aftershocks, listen to radio. Anticipate tsunamis if you're on the coast and quickly go inland or uphill. Also, remember that there very well may be strong aftershocks, that is, additional earthquakes.
5. **Question:** When did the last great subduction-zone earthquake and tsunami hit coastal Oregon?  
**Answer:** a and b — On January 26, A.D. 1700, and about 300 years ago. Scientists have found many lines of evidence for a great (i.e., magnitude 8 and higher) earthquake event about 300 years ago. Evidence includes land subsidence, land uplift, tsunami deposits, liquefaction features, and turbidites, as well as cultural evidence from coastal Native Americans. Studies by a Japanese scientist of the historic record of tsunamis experienced in Japan suggest that a Cascadia event occurred specifically on January 26, 1700. The M 7 Cape Mendocino ("Petrolia") earthquake of April 1992 occurred on the northern Californian coastline about 50 km south of Eureka and was likely a subduction zone earthquake.
6. **Question:** When did the last damaging tsunami hit the Oregon coast?  
**Answer:** c — March 1964. The M 9.2 Prince William Sound Alaska ("Good Friday") earthquake on this date generated a tsunami that hit coastal Oregon (and California). There were several fatalities at Beverly Beach, Oregon, and in Crescent City, California. Low-lying coastal areas that suffered damage due to flooding included Seaside, which suffered the most damage to structures; Newport's Yaquina harbor; and Cannon Beach, which had a bridge collapse.
7. **Question:** Are there active faults near you?  
**Answer:** a — Probably yes, but their locations are not well understood. Earth scientists (seismologists and geologists) have identified *some* faults in Oregon, but certainly not *all* of them. Furthermore, faults that have been identified may or may not be *active*, that is, capable of generating earthquakes. A 1995 report titled "Seismic Design Mapping, State of Oregon," and prepared for the Oregon Department of Transportation includes the most comprehensive *active* fault map for the state. Copies are available in the libraries of the DOGAMI offices in Portland, Baker City, and Grants Pass.
8. **Question:** To protect against loss of life, property, and injury, do the following:  
**Answer:** e — All of the above (vulnerability study, risk study, prioritizing your seismic strengthening needs, and preparing emergency kit and response plan) and follow through with necessary actions. □

## **Appendix 2.**

### **Soil Mercury Analysis**

#### **Introduction**

During the summer of 1995 soil samples were collected in central Lake County, Oregon, from several locations that were previously identified as having recent geothermal activity (Figures 3,4, 6 in report, Table 1 this appendix). The soil samples were later analyzed for mercury to determine if geothermal processes were still active at depth. A total of 435 samples were collected and analyzed, 370 from the north end of Summer Lake in the Picture rock Pass area, and 65 from the north end of Lake Abert in the Sawed Horn area. The procedure of analyzing soil vapor for mercury anomalies as an indicator for active geothermal systems has been used in central Oregon at the Newberry volcanic center in Priest and others 1983.

#### **Sampling Method**

Soil samples were taken at various spacings depending on the transect site, 50, 100, and 200 meter spacings were used. Using a small garden trowel the top 4 to 5 inches of soil was temporarily removed. A representative sample of approximately 500 grams was then excavated and placed into sealing-type plastic bags and labeled according to location. Care was taken to ensure that excessive amounts of organics, especially plant roots, did not become incorporated into the sample so as not to bias the sample with plant material that may have concentrated mercury from the soil. Sample bags were stored out of direct sunlight to inhibit volatilization of mercury from the soil within the bag.

#### **Mercury Sampling Equipment**

For the soil mercury survey a Jerome 431-X Mercury Vapor Analyzer from Arizona Instrument was used. The procedure involved heating a known volume of soil in an enclosed chamber for a determined amount of time, then activating the analyzer which draws a precise volume of air from the chamber across a gold film sensor. The analyzer then calculates the change in electrical resistance across the gold film and displays the concentration of mercury absorbed from the vapor. A standard hot plate was used as the heat source for the test tubes. A temperature of 300 degrees Fahrenheit was determined to be an adequate hot plate temperature to volatilize mercury from the soil samples and to not adversely affect the internal workings of the mercury vapor analyzer. Standard Pyrex test tubes and tygon tubing were also used as part of the analysis apparatus.

### Sample Preparation

A portion of each sample was taken from the sample bag and sieved to remove any plant material, roots, or small rocks. The sieved portion, approximately 20 grams, was placed on paper towels and allowed to dry at room temperature as needed. A .1 gram sample of the sieved soil was placed into a pre-heated test tube which was immediately capped with a test tube head chamber assembly. After the soil was heated for 2 minutes in the sealed test tube, a vapor sample was drawn into the mercury vapor analyzer. Zero air filters were used on top of the test tube head chamber assembly to ensure that air drawn in during sampling was not contaminated by mercury in the lab area. The mercury vapor reading was taken and the next sample was prepared. After sampling, the test tube was removed from the hot plate, soil was dumped out, the tube was allowed to cool and then brushed clean. Once cleaned, the test tubes were returned to the hot plate for pre-heating to ensure that any mercury residue would be volatilized from the tubes before they were used for sampling again.

### Sensitivity

The Jerome 431-X has a rated sensitivity of 0.003 mg/m<sup>3</sup>. The amount of mercury necessary to achieve a minimum (.003 mg/m<sup>3</sup>) reading in a standard air sample aliquot (150 cm<sup>3</sup>) would therefore be 0.00045ug. If all of the mercury in a 0.1 g soil sample were to volatilize at 300 F, a minimum reading should be obtained at a soil mercury concentration of .0045ug/g, or 4.5 ppb. However, replicate analyses by different methods reported by Priest and others (1983) suggest that only about 50% of the total mercury is vaporized at the temperatures used in this study. Therefore we assume the lower detection limit for this study to have been about 10 ppb.

### Conclusions

Results of the soil survey indicate there is no increase of soil mercury due to active geothermal processes in the area where samples were collected. Of the 435 samples that were analyzed there were no anomalous mercury highs observed. We note that mercury studies at Newberry Volcano (Priest and others 1983) which has a documented extensive magma-driven geothermal system showed anomalies up to 90 ppb with local "background" levels of 30 ppb. We are confident that this survey would have located similar anomalies had they been present. This suggests that neither of the sites showing evidence of Quaternary hot springs activity has any current shallow blind geothermal circulation.



Table 1. Soil Mercury Survey Results								Picture Rock Pass Grid							
Grid X	Grid Y	Size	Reading	Grid X	Grid Y	Size	Reading	Grid X	Grid Y	Size	Reading	Grid X	Grid Y	Size	Reading
680000	47650	.1g	.000	680300	47650	.1g	.000	680600	47650	.1g	.000	680900	47650	.1g	.000
680000	47651	.1g	.000	680300	47651	.1g	.000	680600	47651	.1g	.000	680900	47651	.1g	.000
680000	47652	.1g	.000	680300	47652	.1g	.000	680600	47652	.1g	.000	680900	47652	.1g	.000
680000	47653	.1g	.000	680300	47653	.1g	.000	680600	47653	.1g	.000	680900	47653	.1g	.000
680000	47654	.1g	.000	680300	47654	.1g	.000	680600	47654	.1g	.000	680900	47654	.1g	.000
680000	47655	.1g	.000	680300	47655	.1g	.000	680600	47655	.1g	.000	680900	47654	.1g	.000
680000	47656	.1g	.000	680300	47656	.1g	.000	680600	47656	.1g	.000	680900	47654	1.0g	.000
680000	47657	.1g	.000	680300	47657	.1g	.000	680600	47657	.1g	.000	680900	47655	.1g	.000
680000	47658	.1g	.000	680300	47658	.1g	.000	680600	47658	.1g	.000	680900	47655	1.0g	.003
680000	47659	.1g	.000	680300	47659	.1g	.000	680600	47659	.1g	.000	680900	47656	.1g	.000
680000	47660	.1g	.000	680300	47660	.1g	.000	680600	47660	.1g	.000	680900	47657	.1g	.000
680000	47661	.1g	.000	680300	47661	.1g	.000	680600	47661	.1g	.000	680900	47658	.1g	.000
680000	47662	.1g	.000	680300	47662	.1g	.000	680600	47662	.1g	.000	680900	47659	.1g	.000
680000	47663	.1g	.000	680300	47663	.1g	.000	680600	47663	.1g	.000	680900	47660	.1g	.000
680000	47664	.1g	.000	680300	47664	.1g	.000	680600	47664	.1g	.000	680900	47661	.1g	.000
680100	47650	.1g	.000	680400	47650	.1g	.000	680700	47650	.1g	.000	680900	47662	.1g	.000
680100	47651	.1g	.000	680400	47651	.1g	.000	680700	47651	.1g	.000	680900	47663	.1g	.000
680100	47652	.1g	.000	680400	47652	.1g	.000	680700	47652	.1g	.000	680900	47664	.1g	.000
680100	47653	.1g	.000	680400	47653	.1g	.000	680700	47653	.1g	.000	681000	47650	.1g	.000
680100	47654	.1g	.000	680400	47654	.1g	.000	680700	47654	.1g	.000	681000	47651	.1g	.000
680100	47655	.1g	.000	680400	47655	.1g	.000	680700	47655	.1g	.000	681000	47652	.1g	.000
680100	47656	.1g	.000	680400	47656	.1g	.000	680700	47656	.1g	.000	681000	47653	.1g	.000
680100	47657	.1g	.000	680400	47657	.1g	.000	680700	47657	.1g	.000	681000	47654	.1g	.000
680100	47658	.1g	.000	680400	47658	.1g	.000	680700	47658	.1g	.000	681000	47655	.1g	.000
680100	47659	.1g	.000	680400	47659	.1g	.000	680700	47659	.1g	.000	681000	47656	.1g	.000
680100	47660	.1g	.000	680400	47660	.1g	.000	680700	47660	.1g	.000	681000	47657	.1g	.000
680100	47661	.1g	.000	680400	47661	.1g	.000	680700	47661	.1g	.000	681000	47658	.1g	.000
680100	47662	.1g	.000	680400	47662	.1g	.000	680700	47662	.1g	.000	681000	47659	.1g	.000
680100	47663	.1g	.000	680400	47663	.1g	.000	680700	47663	.1g	.000	681000	47660	.1g	.000
680100	47664	.1g	.000	680400	47664	.1g	.000	680700	47664	.1g	.000	681000	47661	.1g	.000
680200	47650	.1g	.000	680500	47650	.1g	.000	680800	47650	.1g	.000	681000	47662	.1g	.000
680200	47651	.1g	.000	680500	47651	.1g	.000	680800	47651	.1g	.000	681000	47663	.1g	.000
680200	47652	.1g	.000	680500	47652	.1g	.000	680800	47652	.1g	.000	681000	47664	.1g	.000
680200	47653	.1g	.000	680500	47653	.1g	.000	680800	47653	.1g	.000	681100	47650	.1g	.000
680200	47654	.1g	.000	680500	47654	.1g	.000	680800	47654	.1g	.000	681100	47651	.1g	.000
680200	47655	.1g	.000	680500	47655	.1g	.000	680800	47655	.1g	.000	681100	47652	.1g	.000
680200	47656	.1g	.000	680500	47656	.1g	.000	680800	47656	.1g	.000	681100	47653	.1g	.000
680200	47657	.1g	.000	680500	47657	.1g	.000	680800	47657	.1g	.000	681100	47654	.1g	.000
680200	47658	.1g	.000	680500	47658	.1g	.000	680800	47658	.1g	.000	681100	47655	.1g	.000
680200	47659	.1g	.000	680500	47659	.1g	.000	680800	47659	.1g	.000	681100	47656	.1g	.000
680200	47660	.1g	.000	680500	47660	.1g	.000	680800	47660	.1g	.000	681100	47657	.1g	.000
680200	47661	.1g	.000	680500	47661	.1g	.000	680800	47661	.1g	.000	681100	47658	.1g	.000
680200	47662	.1g	.000	680500	47662	.1g	.000	680800	47662	.1g	.000	681100	47659	.1g	.000
680200	47663	.1g	.000	680500	47663	.1g	.000	680800	47663	.1g	.000	681100	47660	.1g	.000
680200	47664	.1g	.000	680500	47664	.1g	.000	680800	47664	.1g	.000	681100	47661	.1g	.000
												681100	47662	.1g	.000
												681100	47663	.1g	.000
												681100	47664	.1g	.000

### Appendix 3.

#### Sawed Horn Geology Map Rock Descriptions

- Qp** Holocene beach and lacustrine sediments associated with modern Lake Abert. These are generally fine-grained clay, silt, and sand sediments that occur between Lake Abert and the 4260 ft. contour line. Includes some areas of alkaline marsh and evaporitic deposits, and aeolian deposits.
- Qal** Pleistocene and Holocene? beach and lacustrine deposits higher than Qp and below Qs (4260-4400 ft.). Generally fine sand to fine gravel deposits which mantle the volcanic bedrock surrounding Lake Abert. Gravels composed mainly of basaltic clasts. Sands consist of basaltic and tuffaceous components. Also includes Holocene dune deposits accumulated against the XL Fault escarpment. Playa sediments associated with small enclosed "highland" basins.
- Qt** Late Pleistocene or Holocene? tufa mounds, locally associated with the 4300 ft. elevation contour (15 ft.) White porous calcium carbonate tufa forming mounds of 1-2 meters in height. The base of some tufa mounds is exposed on basaltic bedrock. Sometimes we observe a cemented pavement of rounded beach clasts near the base of these mounds. Also includes veins of dense white crystalline tufa up to 3 cm that locally infill joints in basalt, in the absence of tufa mounds.
- Qs** Coarse sand to gravel shoreline facies associated with the highest Pleistocene pluvial shorelines. Gravel consists mainly of basaltic clasts with some Mr (Rattlesnake AFT). These are mapped topographically above Qal (above 4400 ft.). These deposits drape escarpments obscuring the bedrock lithology.
- Peb** Lower Pliocene? basalt to andesite cones, domes and lavas of Euchre Butte, Jug Mountain, and associated area. Light gray porphyritic basalts and basaltic andesites, containing plagioclase phenocrysts, occasionally glomeroporphyritic. Also includes volcanic breccia near source. The vent areas appear youthful and largely uneroded.
- Mbp** Miocene age basalts which overlie the Rattlesnake AFT at Biscuit Point. A series of flows which exhibit Normal or Reversed magnetic polarity. Gray diktytaxitic, coarsely -vesicular fine-grained mafic lavas. Dominant

phenocryst phase is plagioclase. Basalt flows are generally 5-10 meters in thickness.

- Mr** Miocene (7.05 Ma) Rattlesnake Ash Flow Tuff. Orange-brown pumice and ash-rich Ignimbrite, locally 7 -15 meters thick. Widespread unit and time marker in east-central Oregon. Reverse magnetic polarity.
- Mxl** Miocene basalts which underlie Mr (Rattlesnake AFT) and cropout along the XL Fault escarpment. Light gray diktytaxitic fine-grained lavas. They exhibit Reverse magnetic polarity. Platy-jointed, moderately vesicular lavas with plagioclase and corroded olivine in a diktytaxitic groundmass. Locally observe zeolite and calcite infilled vesicles.
- Mj** Miocene diktytaxitic basalts of Jumbo (Sawed Horn), and interbedded light-orange tuffaceous sediments. Light to steel gray colored very fine-grained basalt and basaltic andesite flows. Flows contain plagioclase (1-2 mm) and orthopyroxene phenocrysts. Finely vesicular. Uppermost flows exhibit Reverse Magnetic Polarity, however does below show Normal Polarity. Flows show weak alteration in places including calcite and zeolite infills of joints and vesicles.
- Msm** Mid-Miocene basalts of Steens Mountain affiliation. Purple to gray colored plagioclase-rich basalt. Porphyritic with plagioclase laths up to 30 mm. Occurs in the southeast part of the mapped region, at the base of Sawed Horn and other bedrock islands.



Figure 1. Study area location map

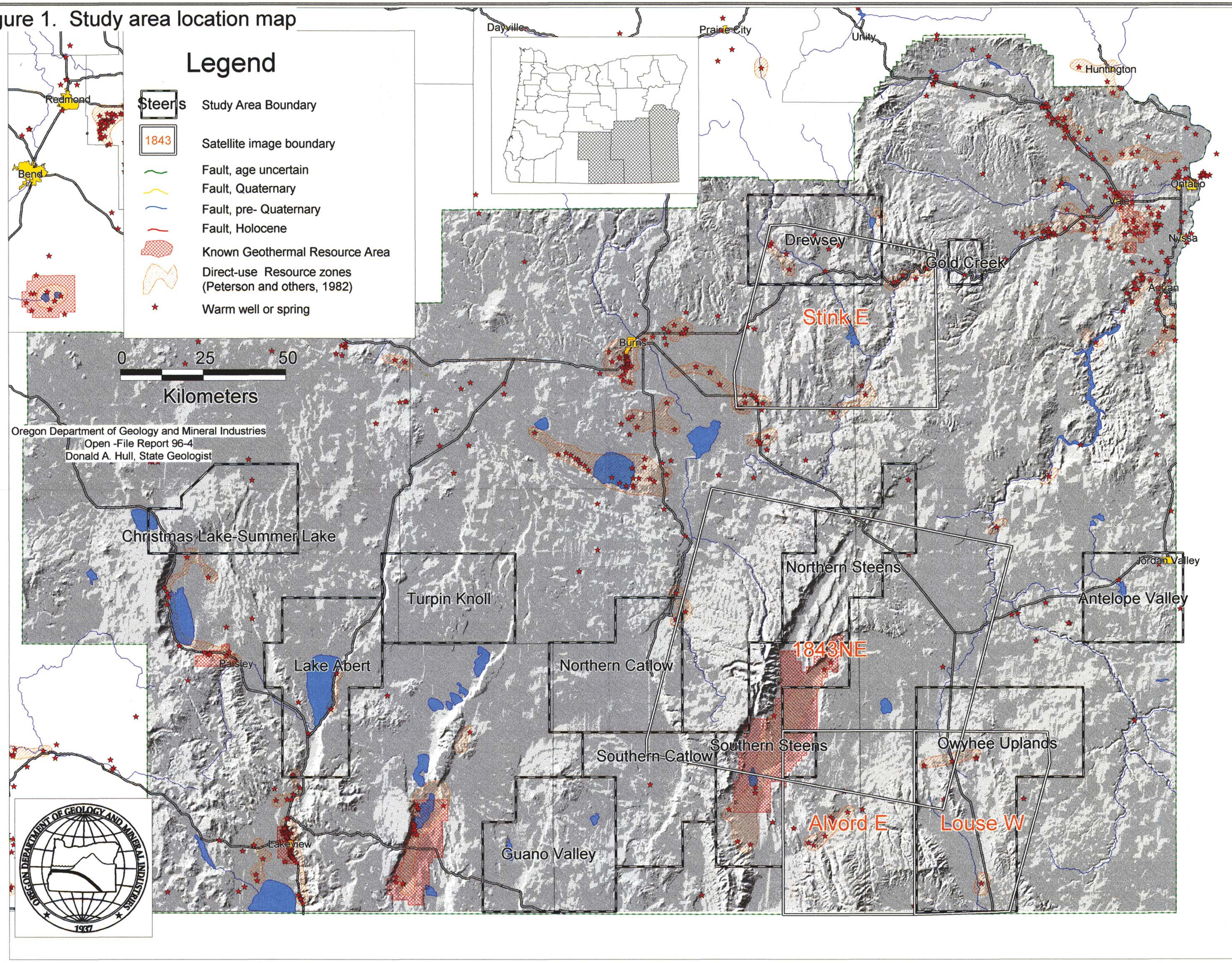









Figure 2.  
Christmas Lake-Summer Lake Study area map

Oregon Department of Geology and Mineral Industries  
Open-File Report OFR-96-4  
Donald A. Hull State Geologist

## Legend

-  Fault, age uncertain
-  Fault, Holocene
-  Warm well or spring, temp in C.
-  Mineral occurrence from MILO
-  Direct-use Resource zones (Peterson and others, 1982)

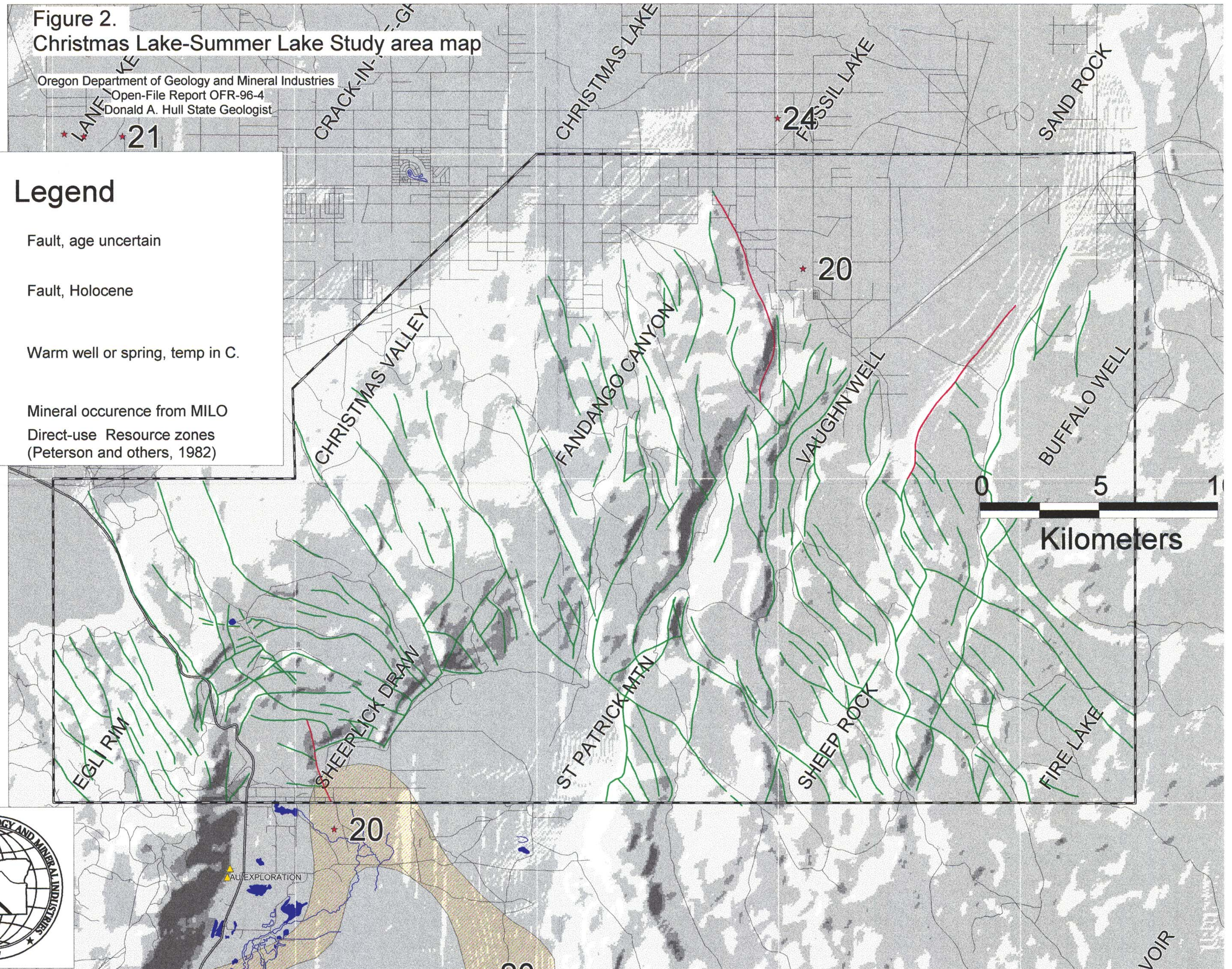
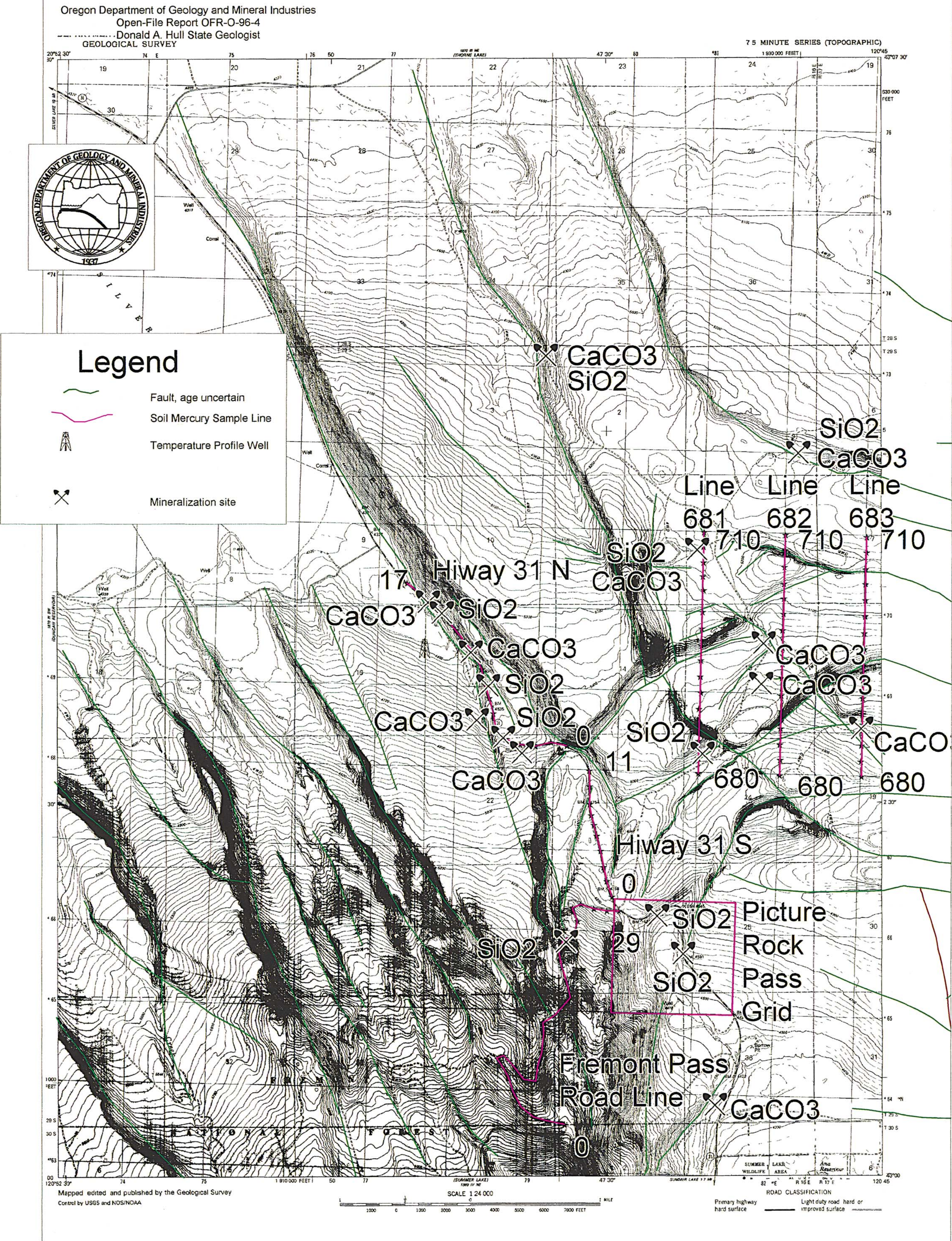




Figure 4. Faulting, mineralization and soil mercury lines in the Picture Rock Pass area, Egli Rim Quadrangle.





**Figure 5. Lake Abert Study Area.**

Oregon Department of Geology and Mineral Industries

Open-File Report OFR-O-96-4

Donald A. Hull State Geologist

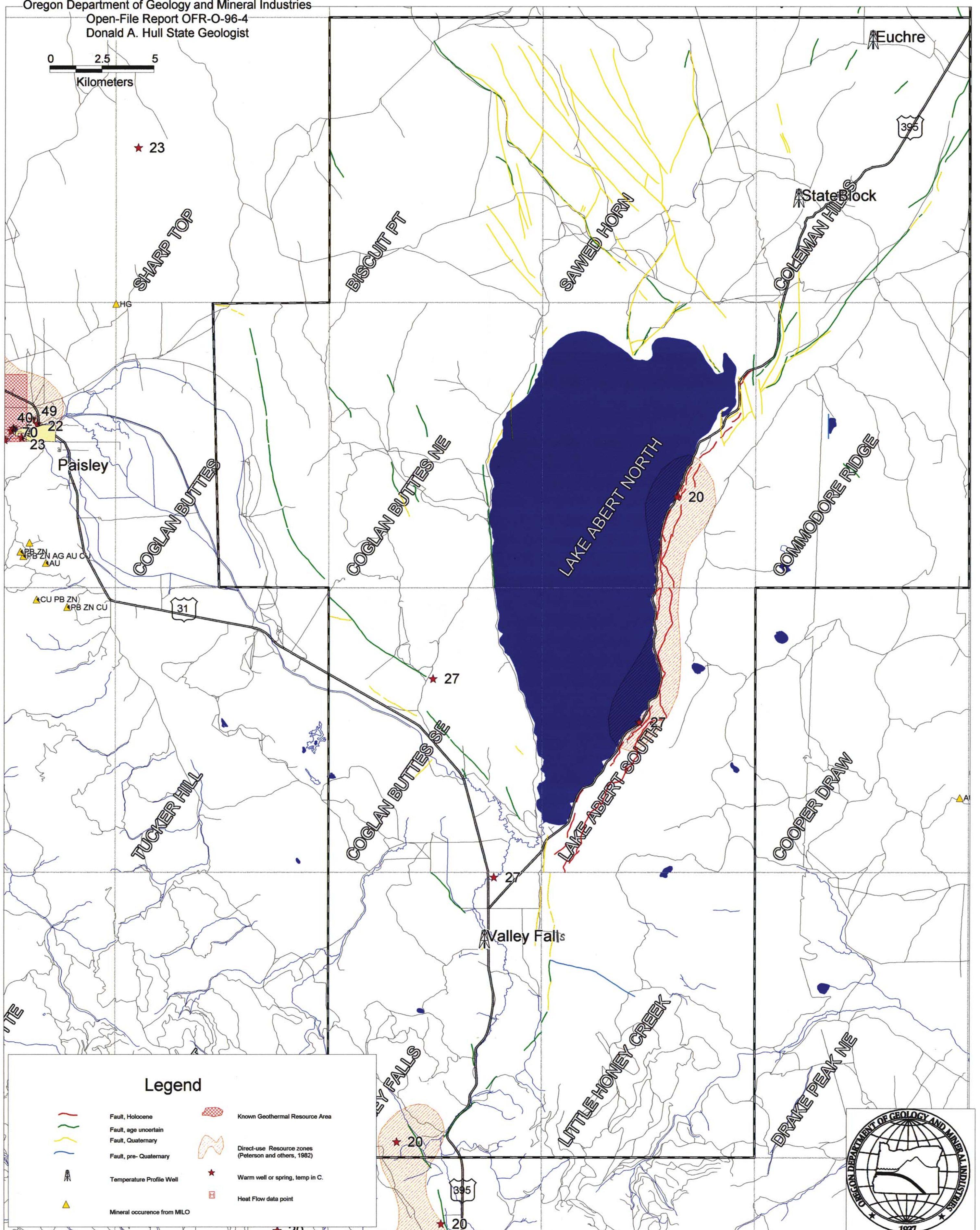




Figure 6 . Preliminary Geologic map of the Sawed Horn area.

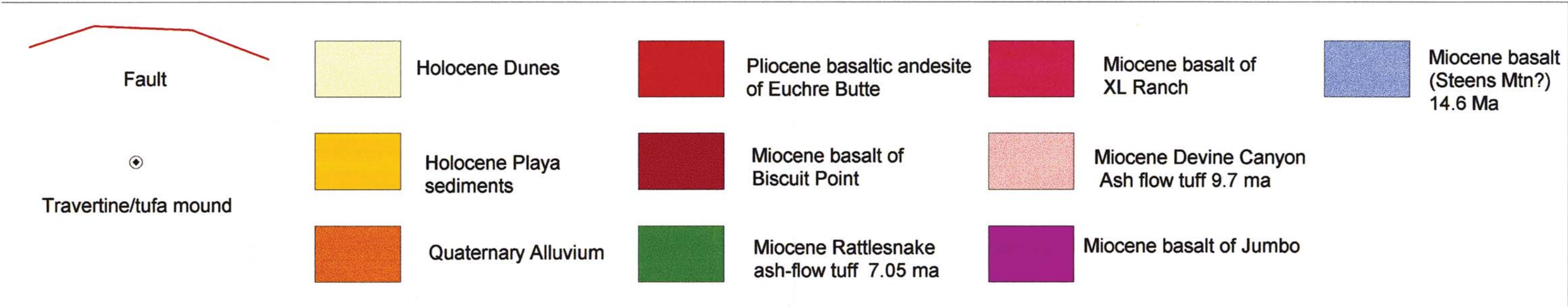




Figure 9. Guano Valley Study area.

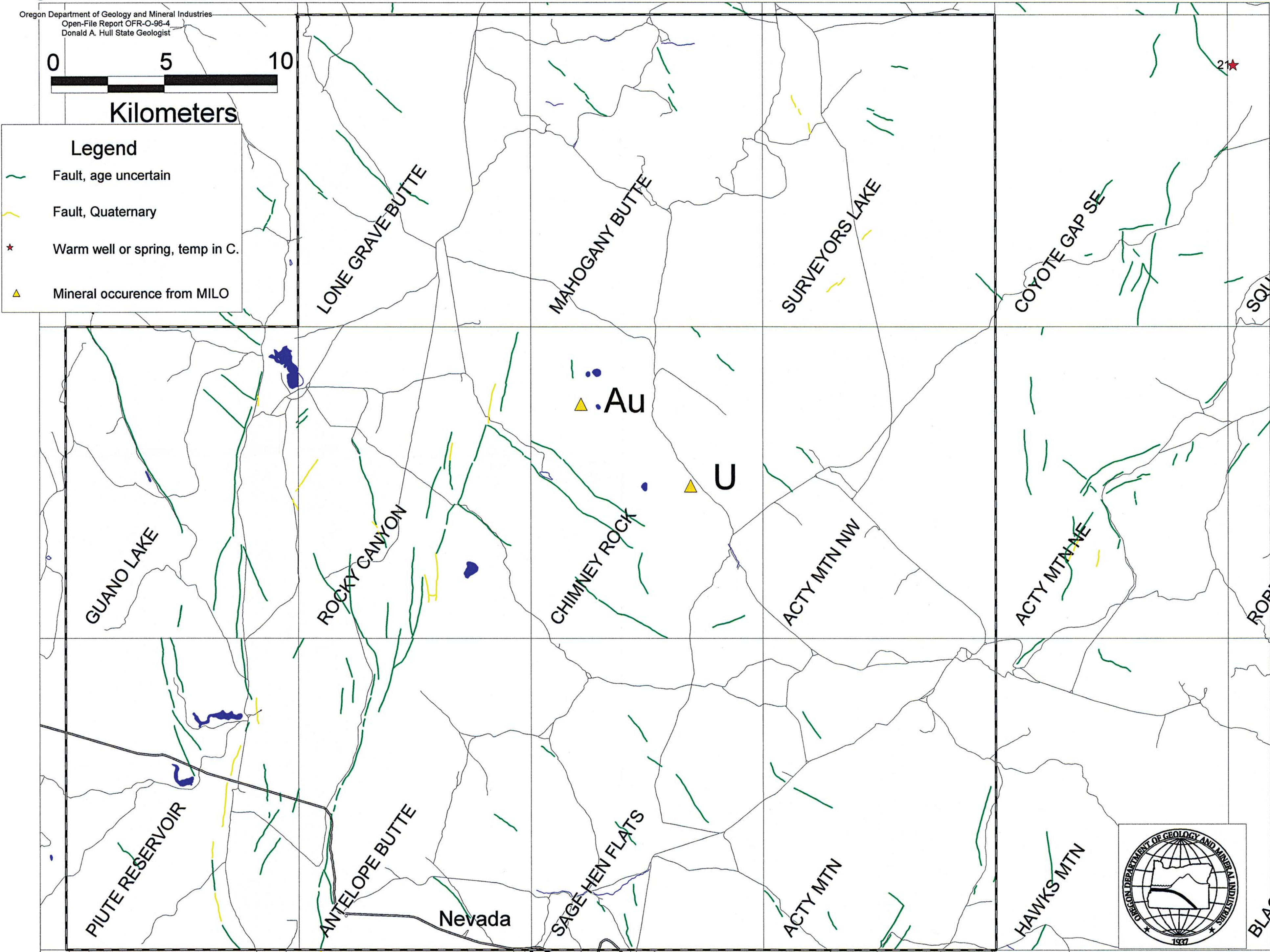




Figure 10. Southern Catlow Valley Study area.

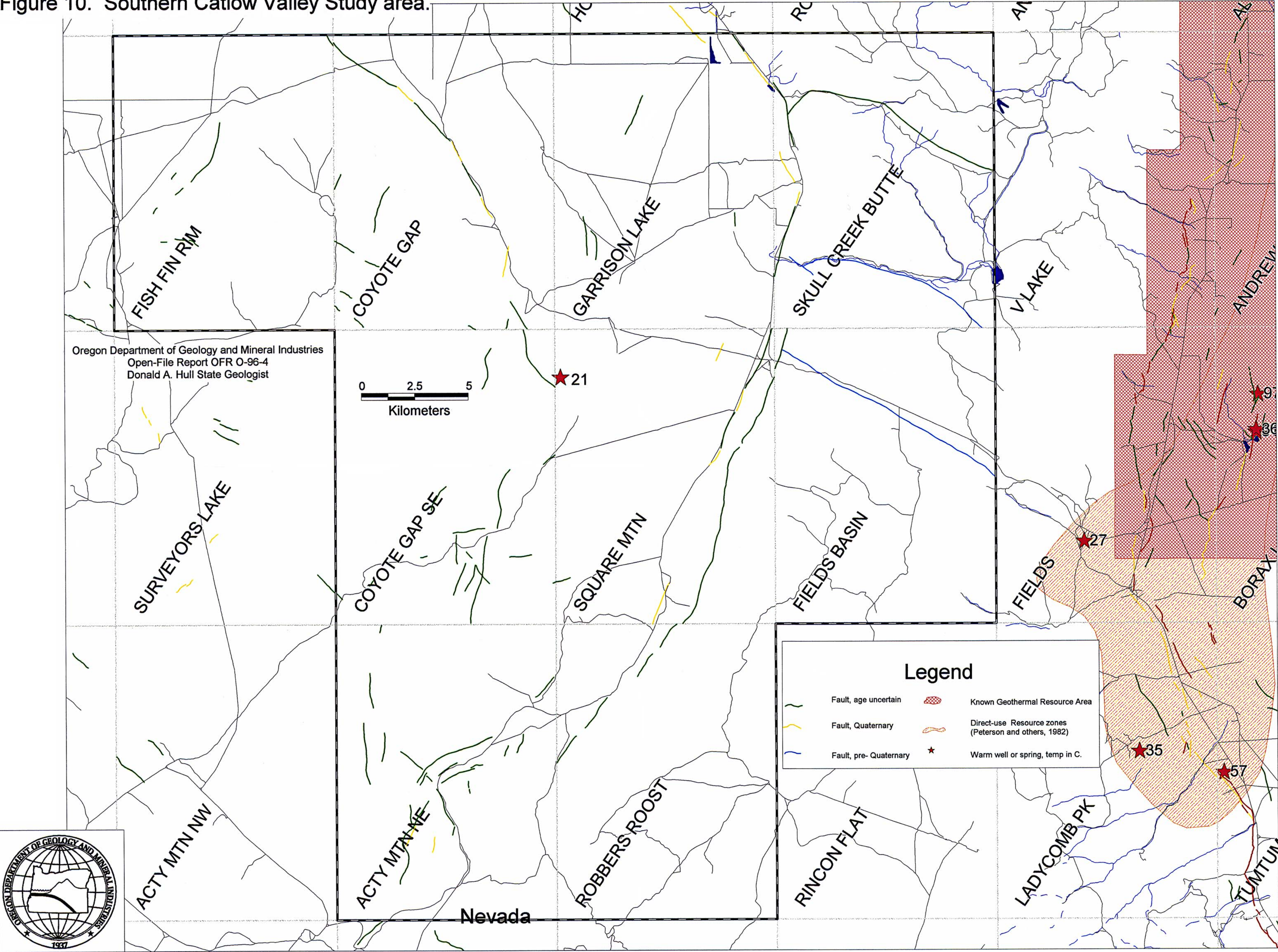
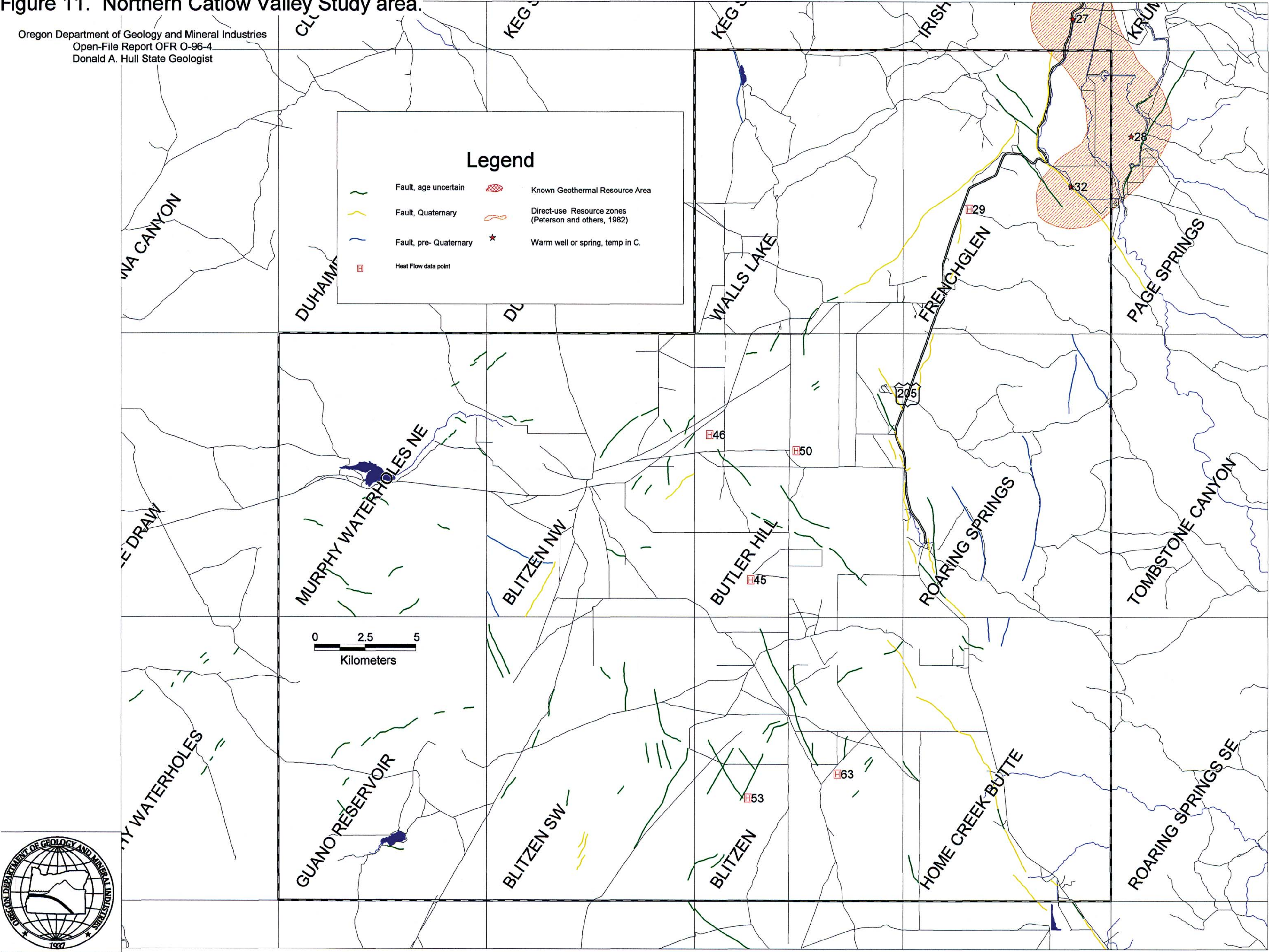




Figure 11. Northern Catlow Valley Study area.

Oregon Department of Geology and Mineral Industries  
Open-File Report OFR O-96-4  
Donald A. Hull State Geologist





[illegible]



Figure 13. Northern Steens study area.

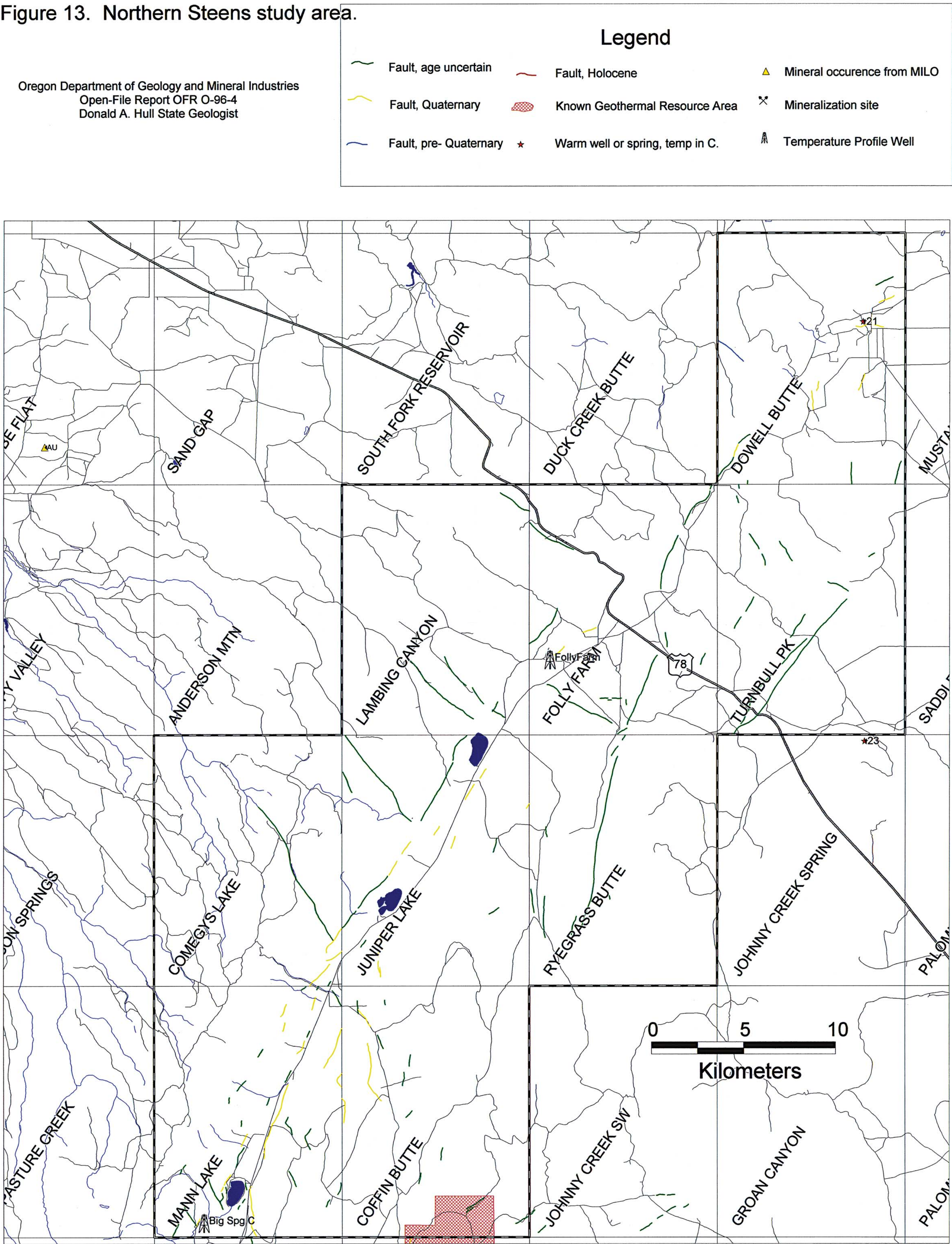




Figure 15. North Half, Owhyee Uplands study area.  
Oregon Department of Geology and Mineral Industries  
Open-File Report OFR O-96-4  
Donald A. Hull State Geologist

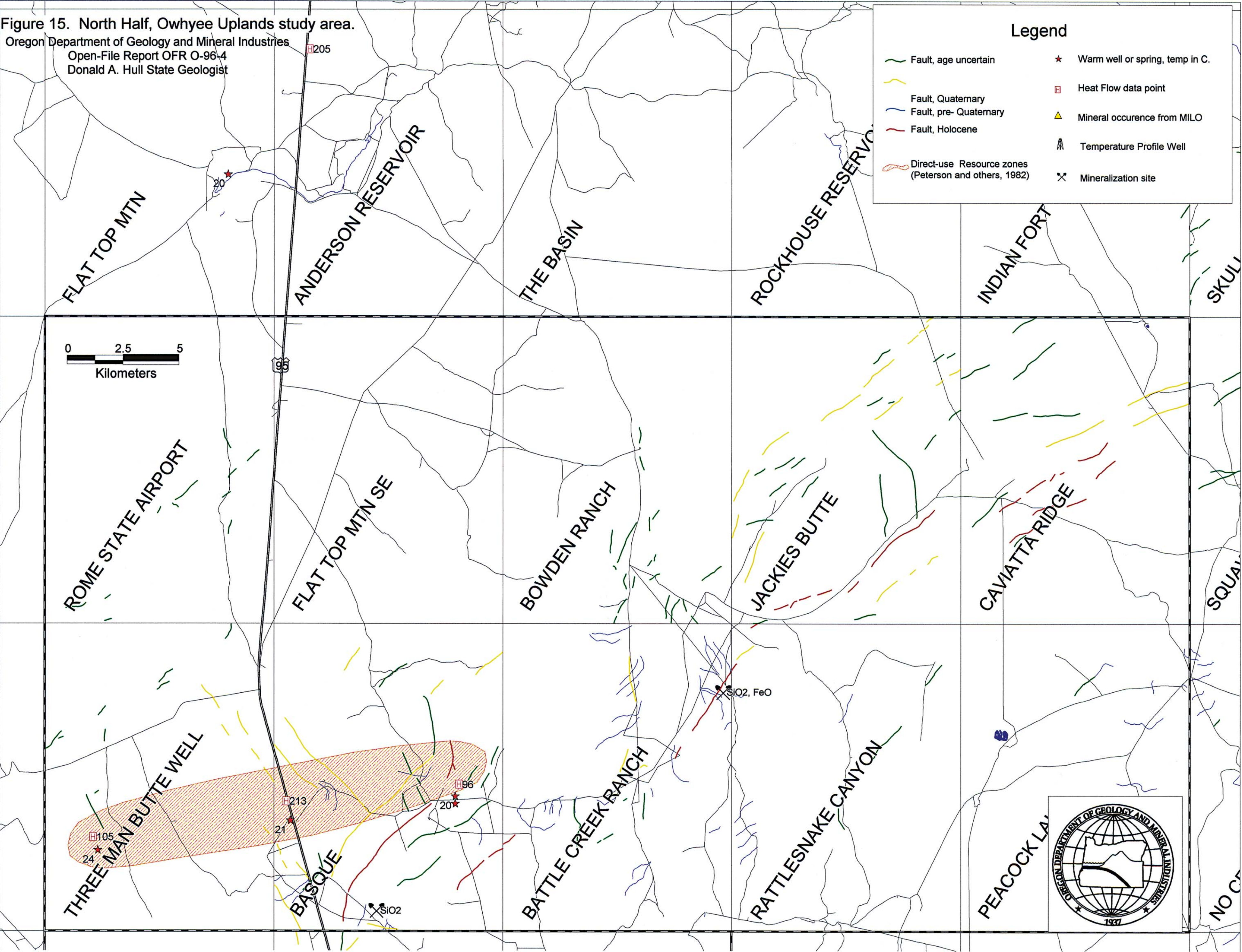




Figure 16. South Half, Owhyee Uplands study area.  
Oregon Department of Geology and Mineral Industries  
Open-File Report OFR O-96-4  
Donald A. Hull State Geologist

